American Heart Association.

Novel Screening Method Identifies PI3Kα, mTOR, and IGF1R as Key Kinases Regulating Cardiomyocyte Survival

Manar Elmadani, MSc; Suleiman Khan, PhD; Olli Tenhunen, MD, PhD; Johanna Magga, PhD; Tero Aittokallio, PhD; Krister Wennerberg, PhD; Risto Kerkelä, MD, PhD

***Background*—**Small molecule kinase inhibitors (KIs) are a class of agents currently used for treatment of various cancers. Unfortunately, treatment of cancer patients with some of the KIs is associated with cardiotoxicity, and there is an unmet need for methods to predict their cardiotoxicity. Here, we utilized a novel computational method to identify protein kinases crucial for cardiomyocyte viability.

***Methods and Results*—**One hundred forty KIs were screened for their toxicity in cultured neonatal cardiomyocytes. The kinase targets of KIs were determined based on integrated data from binding assays. The key kinases mediating the toxicity of KIs to cardiomyocytes were identified by using a novel machine learning method for target deconvolution that combines the information from the toxicity screen and from the kinase profiling assays. The top kinases identified by the model were phosphoinositide 3-kinase catalytic subunit alpha, mammalian target of rapamycin, and insulin-like growth factor 1 receptor. Knockdown of the individual kinases in cardiomyocytes confirmed their role in regulating cardiomyocyte viability.

***Conclusions*—**Combining the data from analysis of KI toxicity on cardiomyocytes and KI target profiling provides a novel method to predict cardiomyocyte toxicity of KIs. **(*J Am Heart Assoc*. 2019;8:e013018. DOI: 10.1161/JAHA.119.013018.)**

Key Words: cardiotoxicity • cell death • pharmacology

Treatment of patients with kinase inhibitors (KIs) has dramatically improved the prognosis of many cancers. Unfortunately, treatment of patients with some of the KIs is associated with cardiotoxicity, and has raised concerns for adverse cardiac effects of kinase inhibition. There are 518 kinases encoded by the kinase genome (kinome).[1] In many cancers, mutations in 1 or several genes encoding kinases can lead to failure in tumor suppression or overexpression of proto-oncogenic proteins. Kinase inhibition in cancer cells can efficiently kill it or stop its growth but, unfortunately, many kinases that drive tumorigenesis are also important for cardiomyocyte survival and function.[2] In addition, most KIs exhibit poor selectivity in their kinase targets because of high homology of ATP pockets across the kinases. Because of the diverse kinase targets found for each KI, many approved KIs are associated with adverse events including cardiomyopathy.[3–5] Currently, among the clinically approved KIs, ponatinib and vandetanib are labeled with the black box warning for cardiovascular implications while for pazopanib, sunitinib, nilotinib, sorafenib, ceritinib, crizotinib, and dasatinib, the cardiovascular events are listed as possible adverse side effects.[5]

Cardiotoxicity has accounted for nearly half of the drug withdrawals, indicating that the predictive value of currently available toxicity screening methods is poor.[6] Cardiotoxicity caused by a KI could result from both (1) on-target toxicity where the kinase that enhances the tumor cell growth is also important for the cardiomyocyte survival; or (2) off-target toxicity where a KI leads to toxicity via inhibition of a kinase not intended to be a target of the drug.[2,3] Off-target toxicity is mainly observed in multitargeted KIs that interact with a wide array of kinase targets. A growing number of patients, many of them with cardiovascular

From the Research Unit of Biomedicine, Department of Pharmacology and Toxicology (M.E., J.M., R.K.) and Department of Oncology and Radiotherapy, Oulu University Hospital (O.T.), University of Oulu, Finland; Institute for Molecular Medicine Finland (FIMM), University of Helsinki, Finland (S.K., T.A., K.W.); Medical Research Center Oulu, Oulu University Hospital and University of Oulu, Finland (R.K.).

Accompanying Data S1, Tables S1 through S3, Figures S1 through S3, and Data Set 1 are available at https://www.ahajournals.org/doi/suppl/10.1161/JAHA.119.013018

Correspondence to: Risto Kerkelä, MD, PhD, Research Unit of Biomedicine, University of Oulu, P.O. Box 5000, FI-90014 Oulu, Finland. E-mail: risto.kerkela@oulu.fi

Received April 25, 2019; accepted August 5, 2019.

Clinical Perspective

What Is New?

- We show that a novel computational method can be used to in vitro screen cardiotoxicity of new kinase inhibitors, a group of widely used anticancer drugs.
- Our data identify novel kinase inhibitor targets, such as dual inhibition of phosphoinositide 3-kinase catalytic subunit alpha and mammalian target of rapamycin, as potential mediators of cardiomyocyte viability and cardiotoxicity.

What Are the Clinical Implications?

- The clinical relevance of this novel assay was supported by identification of well-known cardiotoxic kinase inhibitors.
- Toxicity of dual phosphoinositide 3-kinase catalytic subunit alpha/mammalian target of rapamycin inhibition on cardiomyocytes may bear relevance for future drug design targeting the phosphoinositide 3-kinase catalytic subunit alpha/mammalian target of rapamycin pathway.

comorbidities, are receiving treatments with KIs and currently, predicting cardiotoxicity of KIs in the preclinical phase is a challenge.

Herein, we carried out a systematic approach for identifying kinases, whose inhibition is detrimental for cardiomyocyte viability. We performed analysis of 140 KIs for their ability to induce cardiotoxicity in neonatal rat ventricular cardiomyocytes in vitro. Cardiomyocyte viability was analyzed by measuring the ATP levels in cardiomyocytes after exposure of cells to a 3-log concentration range of each KI for 24 hours. KIs were then analyzed for their kinase targets based on integrated data from binding assays for wild-type kinases (418) considering both on- and off-targets of the KIs. Finally, we developed a novel machine learning method for target deconvolution that combines the information from our toxicity screen and from the kinase profiling assays to identify kinases crucial for cardiomyocyte viability.

Methods

Animal handling and cardiomyocyte isolation were carried out in accordance with University of Oulu institutional guidelines, which conform to the National Research Council (US) Guide for the Care and Use of Laboratory Animals. An expanded methods section is provided in Data S1.

Data Availability

The authors declare that all supporting data are available within the article and its online supplementary files.

Predictive Target Deconvolution

We developed and applied a novel probabilistic machine learning–based predictive target deconvolution approach (PTD). The key assumption of PTD is that by modeling the KI response as an outcome of the target binding affinities, one can deconvolute and identify the key targets that are responsible for the prediction of the response. Specifically, PTD extends sparse linear regression[7] to the case where predictor variables may contain missing values (here, binding affinities, see below). This is achieved by modeling missing predictor variables as parameters of the model that are learned during the inference procedure. As a result, PTD can be considered as a sparse linear regression for noncomplete predictor variables. PTD was used to model the dose–response measurements of a set of KIs as regression outcomes of the corresponding binding affinities. The model is formulated in the Bayesian paradigm as:

$$\boldsymbol{y} \sim \text{Normal}\,(\mathbf{X}\boldsymbol{b}, \sigma)$$

$$\mathbf{X}_u \sim \text{Normal}\,(0, \gamma)$$

$$\boldsymbol{b} \sim \text{Laplace}\,(\alpha)$$

$$\sigma \sim \text{InvGamma}\,(a, b)$$

Here, $\boldsymbol{y}$ forms the dose–response measurements while $\boldsymbol{X}$ are the binding affinities. The outcome variables $\boldsymbol{y}$ are regressed from $\boldsymbol{X}$ with regression coefficients $\boldsymbol{b}$. $\mathbf{X}_u$ represent the unobserved and missing binding affinities. We assume $\boldsymbol{X}_u$ to be centered around zero to match the background data distribution. We also assume normal distributions on $\boldsymbol{y}$ and $\boldsymbol{X}_u$ for simplicity, while varying these could further improve the results. We assume $\boldsymbol{b}$ to have a Laplace prior inspired from sparse linear regression[7] to induce sparsity for the kinase feature selection. Finally, the hyperparameters (α=1, γ=1) are also initialized to induce sparsity in both $\boldsymbol{b}$ and $\mathbf{X}_u$ to match the assumption of sparse feature selection in $\boldsymbol{b}$ and sparsely observed binding affinities in $\boldsymbol{X}_u$. The noise parameter σ is assumed to have a noninformative symmetric prior with shape and rate parameters a,b set to 1. The model was implemented using Gibbs sampling obtaining 200 posterior samples with a thinning factor of 10 and a burnin of 2000 iterations.

To quantify the KI responses, the dose–response curves were summarized using the quantitative drug sensitivity score (DSS).[8] The area under the dose–response curve (AUC) was calculated by fitting a 4-paremeter logistic function to the normalized %inhibition values over the concentration points. A predefined noise threshold (10% inhibition) was further used

in the calculation of the drug sensitivity score (DSS), which classifies each compound with dose–response curved below the threshold as inactive (DSS=0). DSS data from 103 KIs used at maximum 10 μmol/L concentration were used in the PTD analysis. We used both on- and off-target binding affinity profiles to model the polypharmacological effects of KIs. The kinase binding affinities of 132 of the 140 compounds were extracted from the FIMM in-house Drug Target Commons database.[9] For the remaining 8 compounds, the target affinity data were obtained from Davis et al.[10] The integration of the bioactivity profiles was based on the KIBA algorithm.[11] Kinases with affinity values indicating low potency (>1000 nmol/L) were removed as nonrelevant. Furthermore, kinases targeted by ≤3 inhibitors were excluded since they were considered statistically unreliable for PTD inference. This resulted in a total of 295 kinases that were used for modeling the response profiles of the 103 KIs (Data Set 1).

The PTD model was used to infer the top kinases associated with the DSS toxicity responses, where the PTD parameters were estimated using leave-one-out cross-validation. The learned importance scores (regression weights) from each fold were then averaged over the 103-folds to identify the kinases that are robustly linked to the toxicity response. We selected the top-10 kinases based on the regression weights that were found to be consistent across the cross-validation folds using *t* test with Bonferroni multiple-hypothesis correction (differentiating the weights from zero null hypothesis).

Statistical Analysis

Statistical analysis was performed with GraphPad software. Normally distributed data were analyzed with *t* test for 2-sample comparisons. For analysis of 3 or more groups, ANOVA followed by Dunnett's test was used. Differences were considered statistically significant at the level of $P<0.05$. Data are shown as mean±SD.

Results

Effect of KIs on Cardiomyocyte Viability

Measuring the ATP content in viable cells is a widely used approach in cytotoxicity screening applications in vitro. In cardiomyocytes, the number of cells plated showed a linear relationship and were highly correlated with both the ATP measured ($r^2=0.98$, Figure S1A) and the amount of total protein measured at the end of the experiment ($r^2=0.98$, Figure S1B).

For the toxicity analysis, cells were plated at a density of 60 000 cells/well, which is in the linear range of the ATP assay (Figure S1A). After exposure of cardiomyocytes to a 3-log concentration range of each KI for 24 hours, an ATP assay was performed to determine the number of viable cells in culture. Eighty-one of 140 KIs tested showed >10% decrease in cell viability and 27 showed a >30% decrease in cell viability (Figure 1A). The dose–response curves for 33 clinically approved KIs included in the screen are shown in Figure 1B. Twenty-five of the 33 clinically approved KIs included in the study demonstrated a moderate-to-high toxicity to cardiomyocytes. Gefitinib, bosutinib, regorafenib, ponatinib, and midostaurin reduced cardiomyocyte viability by >50% at the maximum concentration tested, while imatinib, erlotinib, sorafenib, sunitinib, dasatinib, lapatinib, nilotinib, pazopanib, axitinib, trametinib, afatinib, ibrutinib, idelalisib, nintedainb, palbociclib, neratinib, binimetinib, dacomitinib, fostamitinib, and everolimus reduced cardiomyocyte viability by 10% to 50% at the maximum concentration tested. The dose–response curves for all KIs analyzed are shown in Table S1.

Identification of Kinases Necessary for Cardiomyocyte Survival

The DSS calculation is based on the integration of the area under the dose–response curve to quantify the summary response intensity. The DSS score is defined within the range of 0 to 50, with close to 0 specifying no response, >5 indicating moderate response, and values close to 50 representing maximally toxic response.[8] DSS score indicated moderate-to-high cardiomyocyte toxicity for 35 of the KIs tested (DSS >5, Figure 2A). Nineteen of the compounds induced low-to-moderate toxicity on cardiomyocytes (2<DSS<5, Figure 2B). DSS values for all the KIs tested are shown in Table S2.

To identify the kinase targets conferring cardiomyocyte toxicity, we analyzed a subset of 103 KIs that were used at maximum 10 μmol/L concentration. Thirty of the KIs had DSS >5 with 10 μmol/L concentration, with expected dose response with 3 and 1 μmol/L concentrations (Figure 2C). A linear regression model was then used to infer the kinases linked with the toxicity response in cardiomyocytes (Figure 2D, Table). The top kinases identified by the model were phosphoinositide 3-kinase catalytic subunit alpha (PI3Kα, p110α), mammalian target of rapamycin (mTOR), and insulin-like growth factor 1 receptor (IGF1R). The rank for Mek1 that has been previously shown to protect the cardiomyocytes from various stresses was 11 (Table).[12] To exclude possible nonspecific toxicities of the kinase inhibitors, we next repeated the PTD model analysis by omitting the toxicity data with the 10 μmol/L KI concentration. Analysis for kinases mediating the toxicity with maximum 3 μmol/L concentration identified the same top 3 kinases (PI3Kα, IGF1R, and mTOR) having the highest regression weights

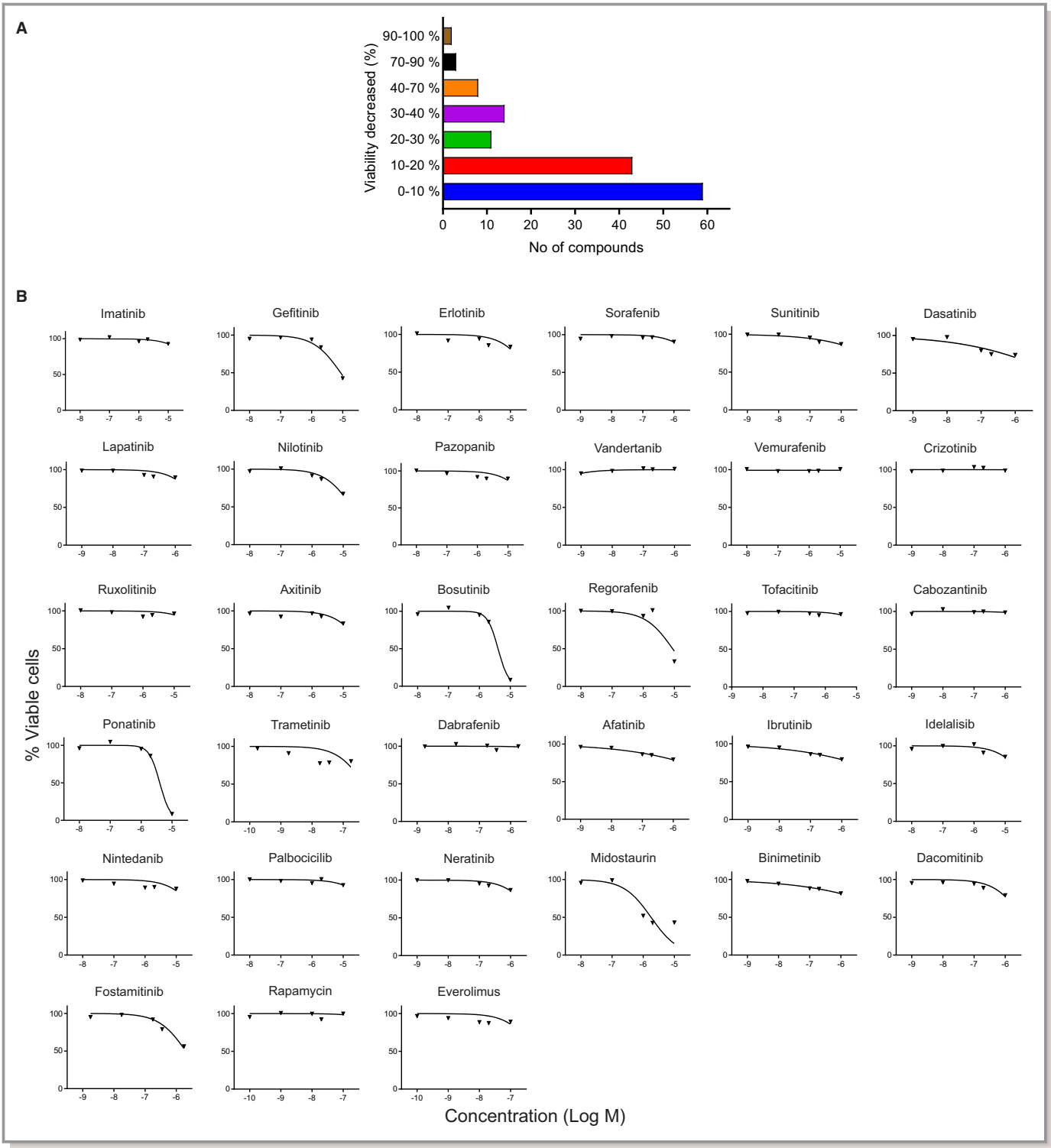

Figure 1. Toxicity of kinase inhibitors (KIs) on cardiomyocytes. Neonatal rat cardiomyocytes were treated with a 3-log concentration range for each kinase inhibitor, and cardiomyocyte viability was assessed by ATP assay. **A**, Classification of cardiomyocyte toxicity of 140 KIs according to percent of viability decreased at maximum concentration. **B**, Dose–response curves for cardiomyocyte viability (% viable cells) of approved KIs analyzed. Each point on the curves represents a mean of 2 replicates.

(Figure 2E). Other kinases identified by both concentration thresholds were B-Raf, PI3K catalytic subunit delta (PI3Kδ), RAF proto-oncogene serine/threonine-protein kinase (Raf-1), PI3K catalytic subunit type 2 beta (PI3K2β), and mitogen-activated protein kinase kinase kinase 7 (MAP3K7 or TAK1).

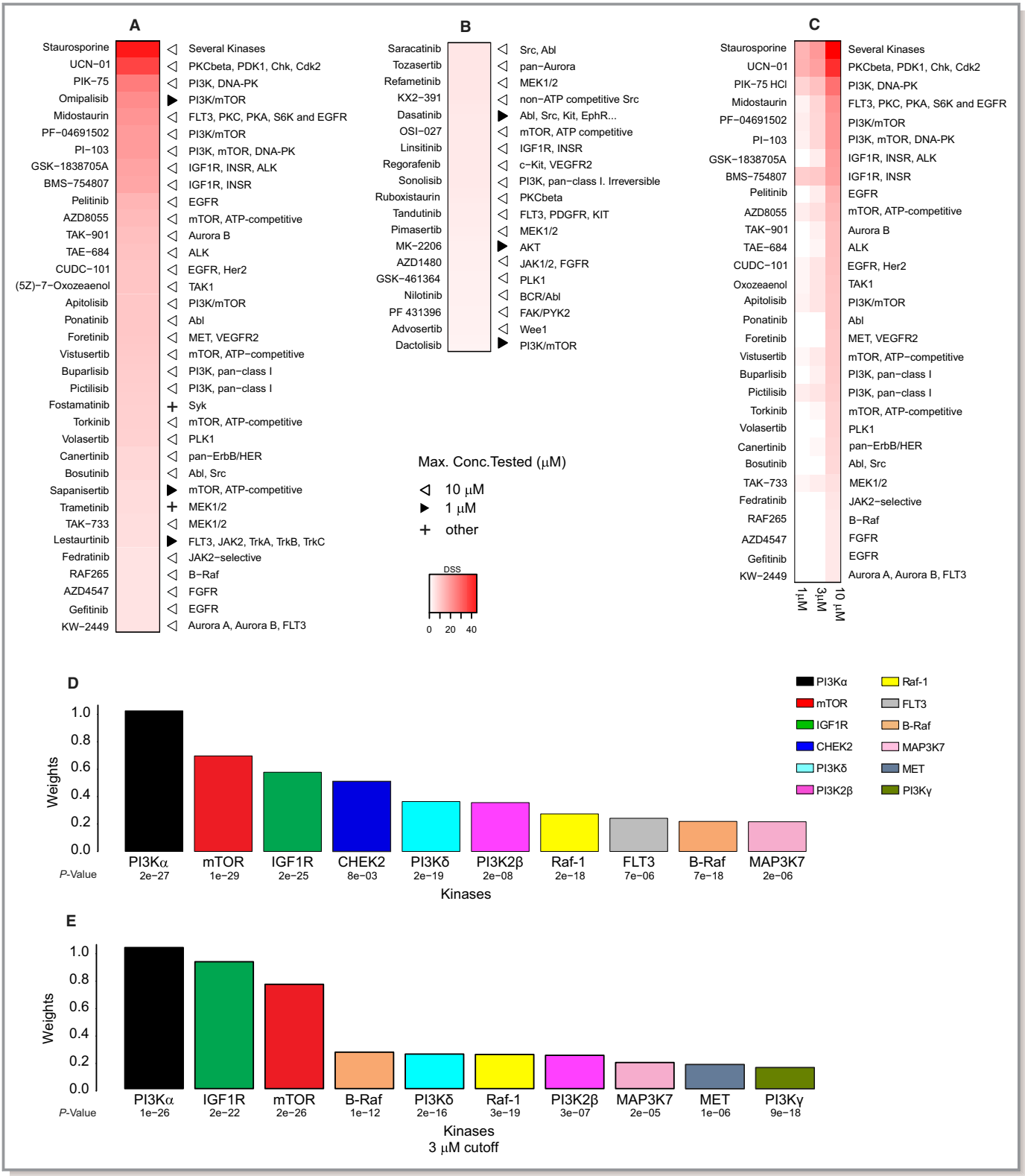

Figure 2. Determination of drug sensitivity score (DSS) and kinases associated with cardiomyocyte survival. **A**, Kinase inhibitors (KIs) with moderate to high toxicity (DSS >5) and their primary kinase targets. **B**, KIs with low-to-moderate toxicity (5>DSS>2) and their primary kinase targets. **C**, DSS and the primary kinase targets for KIs tested at 10 μmol/L maximum concentration. Shown are KIs with DSS>5 and the corresponding DSS value at 3 and 1 μmol/L cutoffs. **D**, Corresponding regression weights of top 10 kinase targets identified by using 10 mmol/L maximum concentration. **E**, Corresponding regression weights of top 10 kinase targets identified by using 3 mmol/L maximum concentration. *P* values are calculated using 1-sided *t* test.

Dual Inhibition of PI3Kα and RICTOR Induces Necrotic Cardiomyocyte Death

mTOR inhibitors analyzed in the study target either mTOR complex 1 (mTORC1) (everolimus and sirolimus) or both mTORC1 and mTORC2 (AZD8055, vistusertib, PP242, sapanasertib, and OSI-027), with markedly higher cardiomyocyte toxicity (DSS >4.3) observed with mTORC1/2 inhibitors. To further investigate the role of PI3Kα, IGF1R, and mTOR, we treated cardiomyocytes with KIs targeting either PI3K, IGF1R, mTOR, or both PI3K and mTOR (dual PI3K/mTOR inhibitors) and analyzed for both ATP levels and necrotic cardiomyocyte death. Cardiomyocytes were incubated with 2-log concentration range of each inhibitor for 24 and 48 hours. Twenty-four-hour incubation of compounds induced a dose-dependent decrease in cardiomyocyte ATP levels, while only PI3K and dual PI3K/mTOR inhibitors induced consistent increase in necrotic cell death (Figure S2 and Table S3). While treatment of cardiomyocytes with some inhibitors (pilaralisib, buparlisib, pictilisib, BMS754807, and omipalisib) induced necrotic cell death with only modest decrease in ATP levels, our data suggest that there is a threshold for the decrease in ATP levels (with ≈50–60% decrease) that results in necrotic cardiomyocyte death (adenylate kinase release). Forty-eight-hour treatment with KIs induced a further decrease in ATP levels, and cardiomyocyte toxicity was observed even with the lowest KI concentration (100 nmol/L) with most of the inhibitors (Figure 3). However, necrotic cell death was consistently observed with only dual PI3K/mTOR inhibitors.

Table. Kinases Regulating Cardiomyocyte Survival Identified by Predictive Target Deconvolution Model

Rank	Targets	Regression Weights	*P* Values
1	PI3Kα	1.025	1.68 E-27
2	mTOR	0.697	9.57 E-30
3	IGF1R	0.578	1.86 E-25
4	CHEK2	0.511	0.008
5	PI3KCδ	0.364	2.30 E-19
6	PI3Kβ	0.356	1.60 E-08
7	Raf-1	0.274	1.55 E-18
8	FLT3	0.242	6.53 E06
9	B-RAF	0.219	6.97 E-18
10	MAP3K7	0.217	1.54 E-06
11	MAP2K1	0.198	2.33 E-05
12	PDGFRA	0.183	1.99 E-12
13	PI3Kγ	0.165	5.65 E-21
14	AURKA	0.154	4.57 E-14
15	MET	0.146	2.07 E-06
16	NTRK3	0.142	1.92 E-12
17	MAP4K5	0.126	1.22 E-11
18	CSNK1D	0.125	2.23 E-05
19	FGFR3	0.117	1.82 E-08
20	AKT1	0.108	0.004
21	MST1R	0.100	6.37 E-06

The kinases ranking is based on the regression weights using the data from 103 kinase inhibitors tested at maximum concentration 10 μmol/L. AKT1 indicates RAC-alpha serine/threonine-protein kinase; AURKA, aurora kinase A; B-RAF, Serine/threonine-protein kinase B-raf; CHEK2, check point kinase 2; CSNK1D, casein kinase 1 delta; FGFR3, fibroblast growth factor receptor 3; FLT3, Fms-related tyrosine kinase 3; IGF1R, insulin-like growth factor-1 receptor; MAPK, mitogen-activated protein kinase; MET, Hepatocyte growth factor receptor; MST1R, macrophage stimulating-1 receptor; mTOR, mammalian target of rapamycin; NTRK3, neurotrophic receptor tyrosine kinase 3; PDGFRA, platelet-derived growth factor receptor alpha; PI3K, phosphoinositide 3-kinase; Raf-1, RAF proto-oncogene serine/threonine-protein kinase.

To confirm the role of the top kinase targets identified on regulating cardiomyocyte viability, we used RNAi to downregulate PI3Kα, IGF1R, and RICTOR (specific protein subunit in the mTORC2 complex) in cardiomyocytes. Quantitative polymerase chain reaction analysis showed that 70 nmol/L siRNA was sufficient to decrease the expression levels of the kinases by ≈50% (Figure S3). It is of note that the decrease in kinase levels achieved by the chosen siRNA concentrations was not complete, but rather mimicked the inhibition achieved with clinically relevant concentration of KIs. Analysis of cardiomyocyte toxicity by ATP assay indicated that PI3Kα and IGF1R silencing modestly reduced cardiomyocyte viability, while RICTOR silencing had no effect (Figure 4A). Interestingly, combined knockdown of the kinases (PI3Kα+IGF1R, PI3Kα+RICTOR, or IGF1R+RICTOR) resulted in toxicity on cardiomyocytes (Figure 4A). Analysis for adenylate kinase release showed that knockdown of individual kinases did not induce necrotic cell death, and only combined silencing of PI3Kα and RICTOR resulted in an increase in AK release (Figure 4B). Taken together, inhibition of either PI3Kα or IGF1R induces a decrease in cellular ATP levels indicative of reduced cardiomyocyte viability. Dual inhibition of PI3K and mTOR decreases cellular ATP levels and induces necrotic cardiomyocyte death.

Discussion

Most of the current data concerning the role of protein kinases in maintenance of normal cardiomyocyte homeostasis are based on studies in mouse knockout models. However, predicting the KI toxicity based entirely on findings in genetically engineered mice may be misleading. Data from studies with germline knockout mice could be confounded by unique developmental roles of the gene. Conditional kinase knockout in cardiomyocytes, on the other hand, results in complete and permanent inhibition of a kinase, which is not achieved with a KI. Knockout models also disrupt protein–protein interactions that will generally not be disrupted with

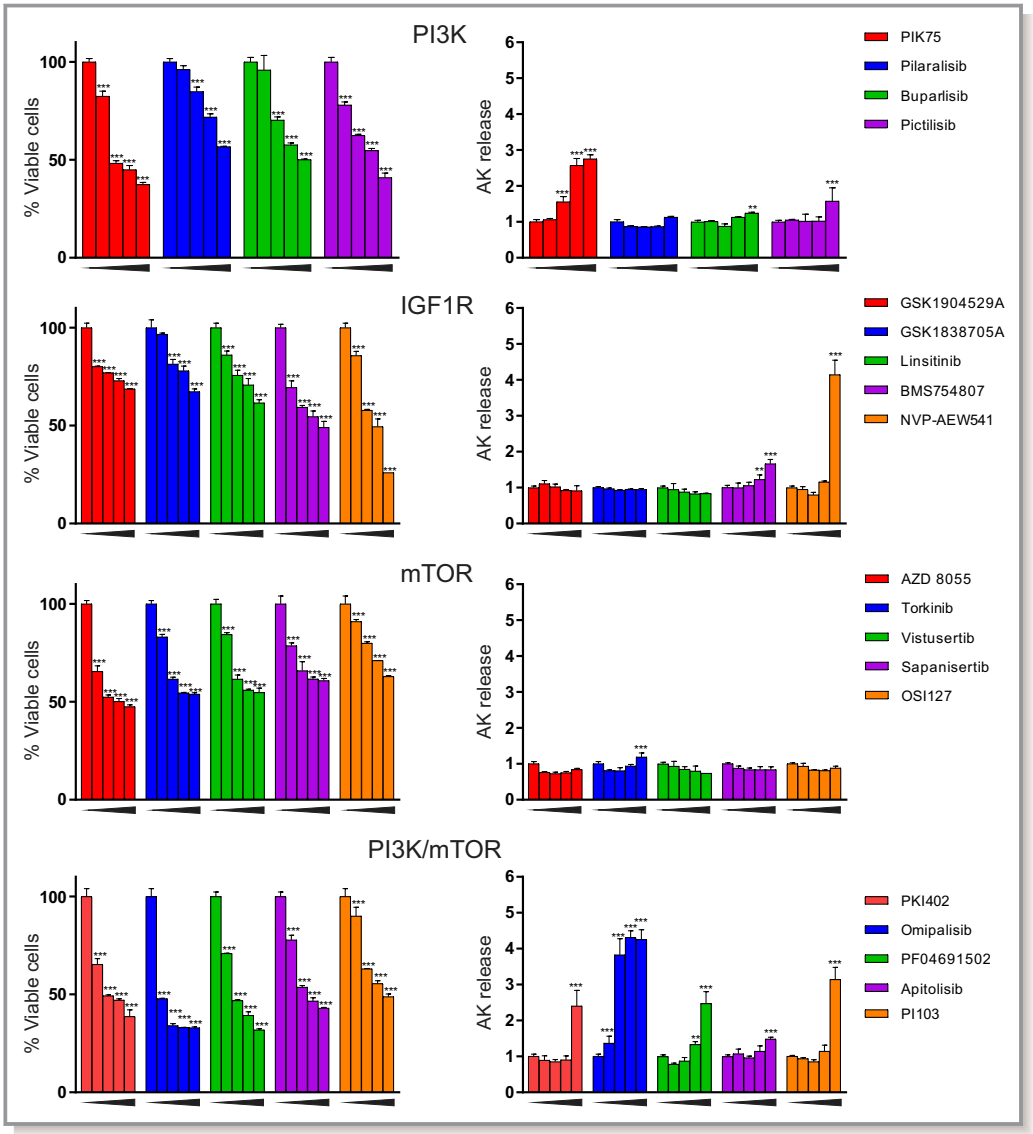

Figure 3. Toxicity of selective PI3K, IGF1R, mTOR, and dual PI3K/mTOR on cardiomyocytes. Neonatal rat cardiomyocytes were treated with 4 different concentrations of each inhibitor for 48 hours. At the end of the experiment, medium samples were collected for adenylate kinase (AK) assay and cells were lysed for measurement of ATP levels. Shown are analyses for cardiomyocyte toxicity by ATP assay (left column) and AK assay (right column). Data for ATP assay are shown as percent of viable cells and for adenylate kinase as fold change vs control. Concentrations from left to right are 0.1, 1, 3, and 10 μmol/L. Data are represented as mean±SD $^{**}P<0.01$; $^{***}P<0.001$ (Dunnett's test).

the drug treatment. This could cause phenotypes in the knockouts that would not be seen with KI treatment.

Currently, there are 50 KIs approved by the US Food and Drug Administration and ≈250 KIs are currently investigated in clinical trials. However, very few of the KIs target only 1 protein within physiologically relevant concentrations.[13,14] The nonclinical development of KIs as well as other anticancer products are mostly performed in line with the ICHS9 regulatory guideline, which only recommends electrocardiographic measurements and appropriate clinical observation to monitor cardiovascular safety.[15] Thus, there is a high unmet need for screening methods that would identify cardiovascular toxicity, and specifically cardiomyocyte toxicity, in earlier phases of anticancer drug development. The neonatal cardiomyocytes provide a unique screening tool to study KI-mediated cardiotoxicity because of their characteristic persistent rhythmic contraction and thus constant requirement for high level of ATP production. It has been shown that, using neonatal cardiomyocytes, many KIs in clinical use including lapatinib, erlotinib, gefitinib, imatinib, sorafenib, sunitinib, and dasatinib induced cardiomyocyte toxicity in a way that correlated with the clinical cardiotoxicity data.[16,17]

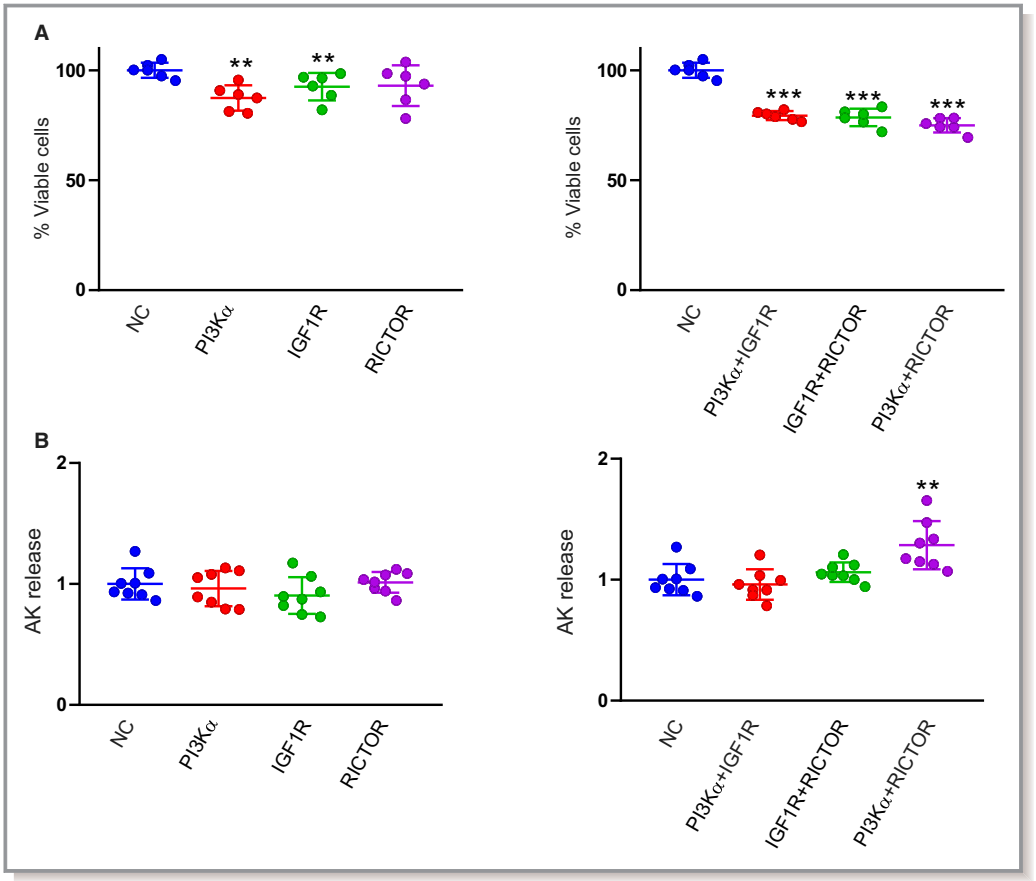

Figure 4. Co-knockdown of PI3Kα and RICTOR induces cardiomyocyte death. Neonatal rat cardiomyocytes were transfected with 70 nmol/L siRNAs targeting PI3Kα, IGF1R, and RICTOR alone, or in combinations. **A**, Analysis of cardiomyocyte viability by ATP assay presented as percent of viable cells. **B**, Analysis of cardiomyocyte necrosis by adenylate kinase (AK) assay presented as fold change compared with control. Scatters represent mean±SD (n=6–8) $^{**}P<0.01$; $^{***}P<0.001$ (*t* test). IGF1R indicates insulin-like growth factor-1 receptor; PI3Kα, phosphoinositide 3-kinase catalytic subunit alpha; RICTOR, Rapamycin-insensitive companion of mTOR.

Apoptosis, necrosis, and autophagy can all contribute to cardiomyocyte death induced by toxic stresses, and the type of cell death following exposure of cardiomyocytes to a given compound cannot be predicted. Thus, analysis for the amount of viable cardiomyocytes following exposure of cardiomyocytes to novel compounds is the most reliable method to detect toxicity. The technique of measuring ATP levels in viable cells is highly sensitive, reproducible, and less vulnerable to false positive results because of the fluorescence of compounds themselves that is commonly observed with fluorescence-based cell viability assays.[18] We found that the ATP assay provides a linear analysis method for measuring cardiomyocyte viability and has a very low threshold for detection of toxicity. Reduction in cardiomyocyte ATP levels may also be indicative of mitochondrial damage/dysfunction that is associated with cardiotoxicity of some KIs.[19,20] In the clinical setting, the decrease in cardiomyocyte ATP levels does not necessarily culminate in cell death, but may manifest as left ventricular dysfunction.

Some aspects need to be taken into account when extrapolating our data from neonatal cardiomyocytes to adult cardiomyocytes. Glycolysis is a predominant source of myocardial ATP production in neonatal cardiomyocytes, whereas the mature heart is mainly aerobic with free fatty acids as the predominant energy substrate.[21] Moreover, cardiomyocytes have proliferative capacity in the neonatal heart, whereas the adult cardiomyocyte proliferation is very limited.[22] Neonatal cardiomyocytes are more resistant to hypoxia[23] and there are differences in calcium signaling between neonatal and adult cardiomyocytes.[24] In the context of cell death, tumor necrosis factor α triggers apoptosis in adult cardiomyocytes but not in neonatal cardiomyocytes.[25] Furthermore, there are some differences in adult and neonatal cardiomyocyte response to toxic stresses. For example, doxorubicin induces calpain-mediated necrotic cell death in

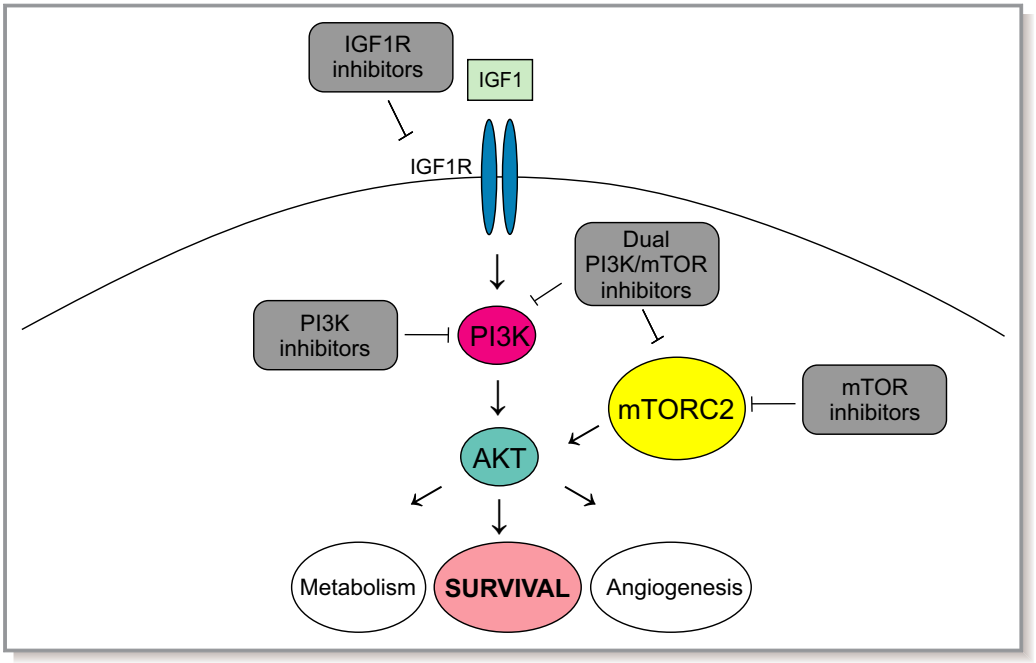

Figure 5. The schematic presentation for the signaling of the top 3 kinases crucial for cardiomyocyte survival. IGF1R is upstream of the prosurvival PI3K/Akt signaling pathway. Dual PI3K/mTOR inhibitors simultaneously inhibit the phosphorylation of Akt and attenuate the prosurvival function of Akt. Akt indicates PKB, Akt serine/threonine kinase; IGF1, insulin-like growth factor I; IGF1R, insulin-like growth factor-1 receptor; mTOR, mammalian target of rapamycin; mTORC2, mammalian target of rapamycin complex 2; PI3K, phosphoinositide 3-kinase.

adult cardiomyocytes, whereas neonatal cardiomyocytes undergo caspase-dependent apoptosis when exposed to doxorubicin.[26,27]

In the current study, the dose–response curve for the toxicity of each inhibitor was summarized using the quantitative DSS, a metric used to determine area under the curve. Compared with other metrics such as IC_{50} and EC_{50}, DSS has the advantage of being robust against sources of technical variability, because it is based on continuous interpolation and integration of multiple dose–response relationships in a high-throughput formulation.[8] By combining the data from DSS determination and KI target profiling, we identified key kinases necessary for cardiomyocyte viability. Specifically, a sparse linear regression was used to infer the kinases linked to the toxicity responses. The concentrations of KIs tested reached maximum free concentration of the compounds in patients.[28] To verify the findings and to exclude possible nonspecific toxicity of the KIs, we also calculated the DSS values for each inhibitor by omitting the highest concentration for each inhibitor. Both of the analyses indicated that PI3Kα, IGF1R, and mTOR are the key top KI targets mediating the toxicity to cardiomyocytes. There are previous data indicating that cardiomyocyte damage correlates with lack of KI specificity.[29] Among the studied KIs in clinical use, bosutinib and ponatinib are least selective,[30] and those are also the KIs with the highest DSS value. However, for KIs in clinical use, lack of target specificity did not correlate with their toxicity to cardiomyocytes (R=0.31; P=0.14). Because cellular ATP levels may decrease without actual cell death, we assessed for rupture of the cell membrane, which is considered a hallmark of necrotic cell death. Our data indicate that only dual inhibition of PI3Kα and mTOR by a KI or kinase knockdown is consistently associated with rupture of the cardiomyocyte cell membrane. The regression analysis also identified Raf-1 and B-Raf among the key mediators of cardiomyocyte viability. Some Raf inhibitors, however, have been shown to paradoxically activate the MAPK pathway in cells bearing oncogenic Ras or elevated upstream receptor signaling.[31–33] The data concerning the role of Raf-1 and B-Raf in regulating cardiomyocyte viability should therefore be interpreted with caution.

Insulin-like growth factor I (IGF1), acting through IGF1R, is one of the key activators of the PI3K pathway, and activation of the PI3K/Akt pathway has been linked to protection from ischemic and toxic cardiac injuries.[34,35] Previously, pharmacological inhibition of PI3Kα has also been shown to abrogate the protective effects of ischemic preconditioning.[36] Mammalian target of rapamycin is found in 2 distinct complexes, mTORC1 and mTORC2. Cardiomyocyte-specific deletion of raptor (specific subunit of mTORC1 complex) disrupted

cardiac function under normal physiological conditions and eventually resulted in heart failure in mice.[37] Cardiomyocyte-specific RICTOR deletion (specific subunit of mTORC2 complex), on the other hand, reduced cardiomyocyte survival and accelerated left ventricular dysfunction in mice in a pressure overload model.[38] Moreover, inhibition of mTORC1 by rapamycin has been shown to protect against cardiac ischemia/reperfusion injury, while dual mTOR inhibitors abolished cardioprotection after ischemic preconditioning.[39,40] While the downstream signaling mechanisms regulating response are not fully elucidated, inhibition of mTORC2 (by RICTOR knockdown) has been shown to reduce Akt phosphorylation, while rapamycin enhances Akt phosphorylation.[38,41]

The PI3K/AKT/mTOR pathway is activated at high frequency in human cancers.[42–44] Given the fact that inhibiting mTORC1 by rapamycin and other rapalogs leads to activation of the PI3K/AKT pathway as a part of its negative feedback mechanism, much attention has been paid to combining mTOR and PI3K inhibitors for additional antitumor activity.[45] Dual inhibition of PI3K and mTOR in human cancers inhibits Akt phosphorylation at 2 distinct phosphorylation sites, resulting in greater antitumor activity.[43] Our current data, however, show that dual inhibition of PI3K and mTOR also results in reduced cardiomyocyte survival (Figure 5). Interestingly, the potency of the 4 dual PI3K/mTOR inhibitors against PI3Kα (Data set 1) highly correlated with the observed DSS value (R=0.82, P=0.14). Development of dual PI3K/mTOR inhibitors has been hampered by adverse effects of compounds, including stomatitis, noninfectious pneumonitis, rash, hyperglycemia, and immunosuppression.[46] Currently, most of the clinical observations of adverse cardiac effects are limited to trials with everolimus or mTOR inhibitors,[47] and cardiovascular effects of the dual PI3K/mTOR inhibition are not well known. Several of the clinically used KIs analyzed in the current study are associated with adverse cardiac effects. We found that 81% of clinically approved KIs included in the study induced toxicity to cardiomyocytes. Use of ponatinib, dasatinib, trametinib, and midostaurin, all highly toxic to cardiomyocytes in the current study, have been associated with development of left ventricular dysfunction and congestive heart failure in patients.[48–50] Our data from isolated cardiomyocytes, however, are not able to detect adverse cardiovascular events stemming from KI toxicity to other resident cardiac cells (eg, endothelial cells).

In summary, we developed here a novel in vitro cardiotoxicity screening method that identifies known cardiotoxic compounds and protective signaling pathways. The method is also readily applicable to other experimental models to identify key kinases mediating cell viability or other biological response. By using this approach, we identify highly adverse effects of PI3Kα/mTOR dual inhibition on cardiomyocytes that may have relevance for future drug design targeting the PI3Kα/mTOR pathway.

Acknowledgments

We thank Marja Arbelius and Kirsi Salo for technical assistance.

Sources of Funding

This work was supported by Academy of Finland grants 131020 and 297094 to Kerkelä and 268505 to Magga, and 296516 to Khan, and by Finnish Foundation for Cardiovascular Research (to Elmadani, Magga, and Kerkelä).

Disclosures

None.

References

1. Roskoski R. A historical overview of protein kinases and their targeted small molecule inhibitors. *Pharmacol Res*. 2015;100:1–23.
2. Lal H, Kolaja KL, Force T. Cancer genetics and the cardiotoxicity of the therapeutics. *J Am Coll Cardiol*. 2013;61:267–274.
3. Force T, Kerkelä R. Cardiotoxicity of the new cancer therapeutics–mechanisms of, and approaches to, the problem. *Drug Discov Today*. 2008;13:778–784.
4. Force T, Kolaja KL. Cardiotoxicity of kinase inhibitors: the prediction and translation of preclinical models to clinical outcomes. *Nat Rev Drug Discov*. 2011;10:111–126.
5. Yeh ETH, Chang H-M. Oncocardiology-past, present, and future: a review. *JAMA Cardiol*. 2016;1:1066–1072.
6. Varga ZV, Ferdinandy P, Liaudet L, Pacher P. Drug-induced mitochondrial dysfunction and cardiotoxicity. *Am J Physiol Heart Circ Physiol*. 2015;309:H1453–H1467.
7. Park T, Casella G. The Bayesian lasso. *J Am Stat Assoc*. 2008;103:681–686.
8. Yadav B, Pemovska T, Szwajda A, Kulesskiy E, Kontro M, Karjalainen R, Majumder MM, Malani D, Murumägi A, Knowles J, Porkka K, Heckman C, Kallioniemi O, Wennerberg K, Aittokallio T. Quantitative scoring of differential drug sensitivity for individually optimized anticancer therapies. *Sci Rep*. 2015;4:5193.
9. Tang J, Tanoli Z-R, Ravikumar B, Alam Z, Rebane A, Vähä-Koskela M, Peddinti G, van Adrichem AJ, Wakkinen J, Jaiswal A, Karjalainen E, Gautam P, He L, Parri E, Khan S, Gupta A, Ali M, Yetukuri L, Gustavsson A-L, Seashore-Ludlow B, Hersey A, Leach AR, Overington JP, Repasky G, Wennerberg K, Aittokallio T. Drug target commons: a community effort to build a consensus knowledge base for drug-target interactions. *Cell Chem Biol*. 2018;25:224–229.
10. Davis MI, Hunt JP, Herrgard S, Ciceri P, Wodicka LM, Pallares G, Hocker M, Treiber DK, Zarrinkar PP. Comprehensive analysis of kinase inhibitor selectivity. *Nat Biotechnol*. 2011;29:1046–1051.
11. Tang J, Szwajda A, Shakyawar S, Xu T, Hintsanen P, Wennerberg K, Aittokallio T. Making sense of large-scale kinase inhibitor bioactivity data sets: a comparative and integrative analysis. *J Chem Inf Model*. 2014;54:735–743.
12. Rose BA, Force T, Wang Y. Mitogen-activated protein kinase signaling in the heart: angels versus demons in a heart-breaking tale. *Physiol Rev*. 2010;90:1507–1546.
13. Bhullar KS, Lagarón NO, McGowan EM, Parmar I, Jha A, Hubbard BP, Rupasinghe HPV. Kinase-targeted cancer therapies: progress, challenges and future directions. *Mol Cancer*. 2018;17:48.
14. Klaeger S, Heinzlmeir S, Wilhelm M, Polzer H, Vick B, Koenig P-A, Reinecke M, Ruprecht B, Petzoldt S, Meng C, Zecha J, Reiter K, Qiao H, Helm D, Koch H, Schoof M, Canevari G, Casale E, Depaolini SR, Feuchtinger A, Wu Z, Schmidt T, Rueckert L, Becker W, Huenges J, Garz A-K, Gohlke B-O, Zolg DP, Kayser G, Vooder T, Preissner R, Hahne H, Tõnisson N, Kramer K, Götze K, Bassermann F, Schlegl J, Ehrlich H-C, Aiche S, Walch A, Greif PA, Schneider S, Felder ER, Ruland J, Médard G, Jeremias I, Spiekermann K, Kuster B. The target landscape of clinical kinase drugs. *Science*. 2017;358:4368.

15. ICH guideline S9 on nonclinical evaluation for anticancer pharmaceuticals, CHMP/ICH/646107/08. European Medicines Agency. Available at: http://www.ema.europa.eu/docs/en_GB/document_library/Scientific_guideline/2010/01/WC500043471.pdf. Accessed September 20, 2019.
16. Hasinoff BB. The cardiotoxicity and myocyte damage caused by small molecule anticancer tyrosine kinase inhibitors is correlated with lack of target specificity. *Toxicol Appl Pharmacol*. 2010;244:190–195.
17. Yang B, Papoian T. Tyrosine kinase inhibitor (TKI)-induced cardiotoxicity: approaches to narrow the gaps between preclinical safety evaluation and clinical outcome. *J Appl Toxicol*. 2012;32:945–951.
18. Ediriweera MK, Tennekoon KH, Samarakoon SR. In vitro assays and techniques utilized in anticancer drug discovery. *J Appl Toxicol*. 2019;39:38–71.
19. Chu TF, Rupnick MA, Kerkela R, Dallabrida SM, Zurakowski D, Nguyen L, Woulfe K, Pravda E, Cassiola F, Desai J, George S, Morgan JA, Harris D, Ismail NS, Chen J-H, Schoen FJ. Cardiotoxicity associated with the tyrosine kinase inhibitor sunitinib. *Lancet*. 2007;370:2011.
20. Kerkelä R, Grazette L, Yacobi R, Iliescu C, Patten R, Beahm C, Walters B, Shevtsov S, Pesant S, Clubb FJ, Rosenzweig A, Salomon RN, Van Etten RA, Alroy J, Durand J-B, Force T. Cardiotoxicity of the cancer therapeutic agent imatinib mesylate. *Nat Med*. 2006;12:908–916.
21. Lopaschuk GD, Spafford MA, Marsh DR. Glycolysis is predominant source of myocardial ATP production immediately after birth. *Am J Physiol*. 1991;261:H1698–H1705.
22. Yutzey KE. Cardiomyocyte proliferation. *Circ Res*. 2017;120:627–629.
23. Kang PM, Haunstetter A, Aoki H, Usheva A, Izumo S. Morphological and molecular characterization of adult cardiomyocyte apoptosis during hypoxia and reoxygenation. *Circ Res*. 2000;87:118–125.
24. Poindexter BJ, Smith JR, Buja LM, Bick RJ. Calcium signaling mechanisms in dedifferentiated cardiac myocytes: comparison with neonatal and adult cardiomyocytes. *Cell Calcium*. 2001;30:373–382.
25. Krown KA, Page MT, Nguyen C, Zechner D, Gutierrez V, Comstock KL, Glembotski CC, Quintana PJ, Sabbadini RA. Tumor necrosis factor alpha-induced apoptosis in cardiac myocytes. Involvement of the sphingolipid signaling cascade in cardiac cell death. *J Clin Invest*. 1996;98:2854–2865.
26. Lim CC, Zuppinger C, Guo X, Kuster GM, Helmes M, Eppenberger HM, Suter TM, Liao R, Sawyer DB. Anthracyclines induce calpain-dependent titin proteolysis and necrosis in cardiomyocytes. *J Biol Chem*. 2004;279:8290–8299.
27. Konorev EA, Vanamala S, Kalyanaraman B. Differences in doxorubicin-induced apoptotic signaling in adult and immature cardiomyocytes. *Free Radic Biol Med*. 2008;45:1723–1728.
28. Liston DR, Davis M. Clinically relevant concentrations of anticancer drugs: a guide for nonclinical studies. *Clin Cancer Res*. 2017;23:3489–3498.
29. Hasinoff BB, Patel D. The lack of target specificity of small molecule anticancer kinase inhibitors is correlated with their ability to damage myocytes in vitro. *Toxicol Appl Pharmacol*. 2010;249:132–139.
30. Uitdehaag JCM, de Roos JADM, van Doornmalen AM, Prinsen MBW, de Man J, Tanizawa Y, Kawase Y, Yoshino K, Buijsman RC, Zaman GJR. Comparison of the cancer gene targeting and biochemical selectivities of all targeted kinase inhibitors approved for clinical use. *PLoS One*. 2014;9:e92146.
31. Hatzivassiliou G, Song K, Yen I, Brandhuber BJ, Anderson DJ, Alvarado R, Ludlam MJC, Stokoe D, Gloor SL, Vigers G, Morales T, Aliagas I, Liu B, Sideris S, Hoeflich KP, Jaiswal BS, Seshagiri S, Koeppen H, Belvin M, Friedman LS, Malek S. RAF inhibitors prime wild-type RAF to activate the MAPK pathway and enhance growth. *Nature*. 2010;464:431–435.
32. Heidorn SJ, Milagre C, Whittaker S, Nourry A, Niculescu-Duvas I, Dhomen N, Hussain J, Reis-Filho JS, Springer CJ, Pritchard C, Marais R. Kinase-dead BRAF and oncogenic RAS cooperate to drive tumor progression through CRAF. *Cell*. 2010;140:209–221.
33. Poulikakos PI, Zhang C, Bollag G, Shokat KM, Rosen N. RAF inhibitors transactivate RAF dimers and ERK signalling in cells with wild-type BRAF. *Nature*. 2010;464:427–430.
34. Riehle C, Abel ED. Insulin signaling and heart failure. *Circ Res*. 2016;118:1151–1169.
35. Rossello X, Yellon DM. The RISK pathway and beyond. *Basic Res Cardiol*. 2017;113:2.
36. Rossello X, Riquelme JA, He Z, Taferner S, Vanhaesebroeck B, Davidson SM, Yellon DM. The role of PI3Kα isoform in cardioprotection. *Basic Res Cardiol*. 2017;112:66.
37. Shende P, Plaisance I, Morandi C, Pellieux C, Berthonneche C, Zorzato F, Krishnan J, Lerch R, Hall MN, Rüegg MA, Pedrazzini T, Brink M. Cardiac raptor ablation impairs adaptive hypertrophy, alters metabolic gene expression, and causes heart failure in mice. *Circulation*. 2011;123:1073–1082.
38. Shende P, Xu L, Morandi C, Pentassuglia L, Heim P, Lebboukh S, Berthonneche C, Pedrazzini T, Kaufmann BA, Hall MN, Rüegg MA, Brink M. Cardiac mTOR complex 2 preserves ventricular function in pressure-overload hypertrophy. *Cardiovasc Res*. 2016;109:103–114.
39. Sciarretta S, Forte M, Frati G, Sadoshima J. New insights into the role of mTOR signaling in the cardiovascular system. *Circ Res*. 2018;122:489–505.
40. Yano T, Ferlito M, Aponte A, Kuno A, Miura T, Murphy E, Steenbergen C. Pivotal role of mTORC2 and involvement of ribosomal protein S6 in cardioprotective signaling. *Circ Res*. 2014;114:1268–1280.
41. Wang X, Yue P, Kim YA, Fu H, Khuri FR, Sun S-Y. Enhancing mammalian target of rapamycin (mTOR)–targeted cancer therapy by preventing mTOR/raptor inhibition-initiated, mTOR/rictor-independent Akt activation. *Cancer Res*. 2008;68:7409–7418.
42. Lee JJ, Loh K, Yap Y-S. PI3K/Akt/mTOR inhibitors in breast cancer. *Cancer Biol Med*. 2015;12:342–354.
43. Stratikopoulos EE, Parsons RE. Molecular pathways: targeting the PI3K pathway in cancer-BET inhibitors to the rescue. *Clin Cancer Res*. 2016;22:2605–2610.
44. van der Heijden MS, Bernards R. Inhibition of the PI3K pathway: hope we can believe in? *Clin Cancer Res*. 2010;16:3094–3099.
45. Dufour M, Dormond-Meuwly A, Demartines N, Dormond O. Targeting the mammalian target of rapamycin (mTOR) in cancer therapy: lessons from past and future perspectives. *Cancers (Basel)*. 2011;3:2478–2500.
46. Chia S, Gandhi S, Joy AA, Edwards S, Gorr M, Hopkins S, Kondejewski J, Ayoub JP, Califaretti N, Rayson D, Dent S. Novel agents and associated toxicities of inhibitors of the pi3k/Akt/mtor pathway for the treatment of breast cancer. *Curr Oncol*. 2015;22:33.
47. Hall PS, Harshman LC, Srinivas S, Witteles RM. The frequency and severity of cardiovascular toxicity from targeted therapy in advanced renal cell carcinoma patients. *JACC Heart Fail*. 2013;1:72–78.
48. Flaherty KT, Robert C, Hersey P, Nathan P, Garbe C, Milhem M, Demidov LV, Hassel JC, Rutkowski P, Mohr P, Dummer R, Trefzer U, Larkin JMG, Utikal J, Dreno B, Nyakas M, Middleton MR, Becker JC, Casey M, Sherman LJ, Wu FS, Ouellet D, Martin A-M, Patel K, Schadendorf D. Improved survival with MEK inhibition in BRAF-mutated melanoma. *N Engl J Med*. 2012;367:107–114.
49. Pun SC, Neilan TG. Cardiovascular side effects of small molecule therapies for cancer: table 1. *Eur Heart J*. 2016;37:2742–2745.
50. Strati P, Kantarjian H, Ravandi F, Nazha A, Borthakur G, Daver N, Kadia T, Estrov Z, Garcia-Manero G, Konopleva M, Rajkhowa T, Durand M, Andreeff M, Levis M, Cortes J. Phase I/II trial of the combination of midostaurin (PKC412) and 5-azacytidine for patients with acute myeloid leukemia and myelodysplastic syndrome. *Am J Hematol*. 2015;90:276–281.

SUPPLEMENTAL MATERIAL

Data S1.

Supplemental Methods

Reagents

A panel of 118 inhibitors was obtained from Institute for Molecular Medicine Finland (FIMM). Another panel of 22 inhibitors was purchased from Selleckchem. CellTiter-Glo Luminescent Cell Viability Assay was purchased form Promega. The adenylate kinase bioassay kit (Toxilight) was purchased from Lonza.

Isolation of cardiomyocytes

Collagenase dissociation method was used for isolation of neonatal rat ventricular cardiomyocytes. 2-4 days old rat pups were decapitated, the thoracic cavity was opened, and the isolated ventricles were perfused with 1% PBS then cut into pieces for digestion in collagenase solution (CLS-2 2 g/l and CaCl2 50 µM in PBS) at 37°C. The cell suspension was filtered through 100 µm nylon mesh. To wash collagenase out, the suspension was centrifuged for 5 min at 175 g and resuspended in Dulbecco's modified Eagle's medium (DMEM) supplemented with 10% FBS and antibiotics (100 IU/ml penicillin and 100 mg/l streptomycin). Centrifugation and resuspension were repeated once to enhance washing. Pre-plating in 100 mm dishes for 2h at 37°C in humidified air with 5% CO2 was used to get rid of non-myocyte cells fraction. The non-attaching cardiomyocytes were collected, and viable cells were counted using a Bürker hemocytometer. Cells were plated at a density of 60000 cells/well using 96 wells plate with clear bottom in 10% FBS DMEM cell culture medium for 24h to allow cardiomyocytes to attach after which medium was changed into 2% FBS Ham's F10 Nutrient Mix (supplemented with antibiotics) for another 24h before experiment started.

RNA interference

Specific phosphatidylinositol 4,5-bisphosphate 3-kinase catalytic subunit alpha isoform (PI3Kα, p110α), Rapamycin-insensitive companion of mTOR (RICTOR), insulin-like growth factor 1 receptor (IGF1R) siRNAs, and negative control siRNA from (ThermoFisher) were transfected into the cardiomyocytes using Lipofectamine2000 (Invitrogen) as transfection reagent. Cells were incubated in OPTI-mem (Invitrogen) for 18 h, and thereafter the cells were incubated in Ham's F10 Nutrient Mix supplemented with 2% fetal bovine serum.

RNA analysis

The RNA was extracted from cardiomyocytes with Trizol reagent following the manufacturer's protocol (Invitrogen, Life Technologies). cDNA was analyzed by quantitative real-time polymerase chain reaction (RT-PCR) using the SYBR Green Master Mix (ThermoFisher) on an ABI 7300 sequence detection system (Applied biosystems, Life Technologies). Oligonucleotide primers used for real time quantitative RT-PCR: PI3Kα forward, CACGACCATCTTCGGGTG, and reverse: GGGAGTAAACATTCCACTAGGA;

IGF1R forward, GCCCCGATATGCTGTTTG, and reverse: ACTGGGCTCCATCTCATCC; RICTOR forward: GACACCATCACCATGAAGG, and reverse: ACCATAGACCTAACTGAGGA; 18S forward: CGCCGCTAGAGGTGAAATTC, and reverse: CCAGTCGGCATCGTTTATGG.

Table S1. Dose response curves of all KIs included in the screen. Quantification of cytotoxicity was done using CellTiterGlo assay after treatment of neonatal cardiomyocytes with five different concentrations of each kI. Data are mean of two replicates. Inhibitors are shown in alphabetical order. Prism (GraphPad) was used for curve fitting.

Inhibitor	Graph
(5Z)-7-Oxozeaenol (≤10 µM)	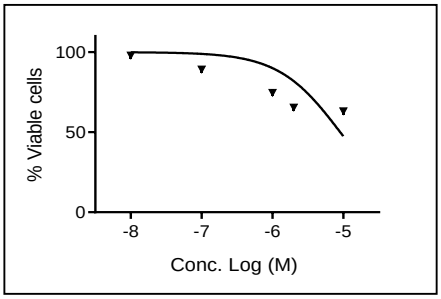
Advosertib (MK-1775) (≤10 µM)	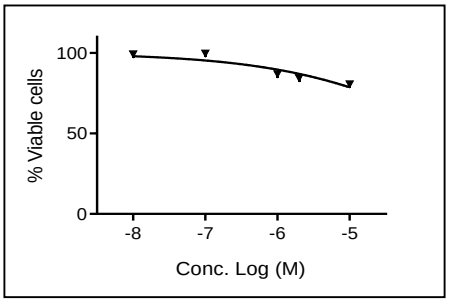
Afatinib (BIBW2992)(≤ 1 µM)	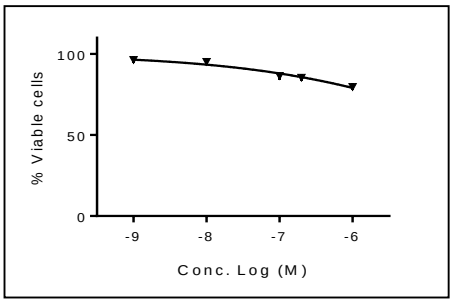
Alisertib (MLN8237) (≤10 µM)	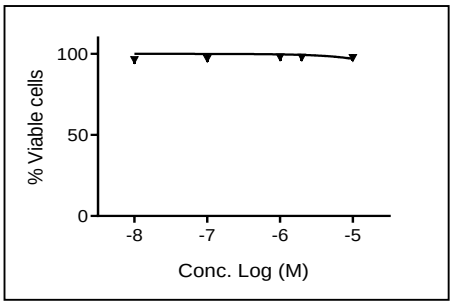

Apitolisib (GDC-0980, RG7422)(≤10 µM)	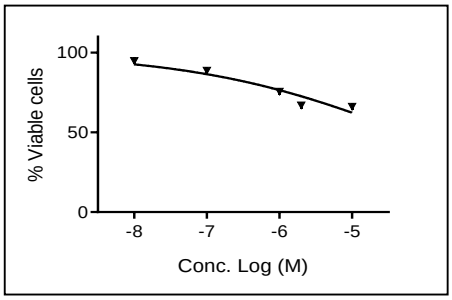
AT9283 (≤1 µM)	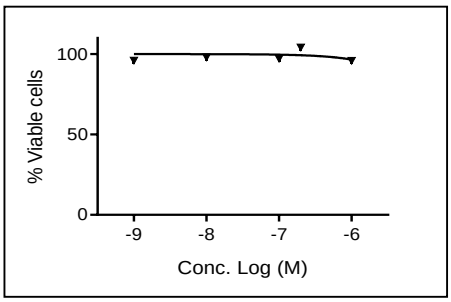
Axitinib (≤10 µM)	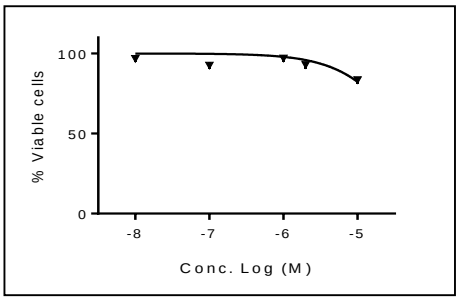
AZ 3146 (≤10 µM)	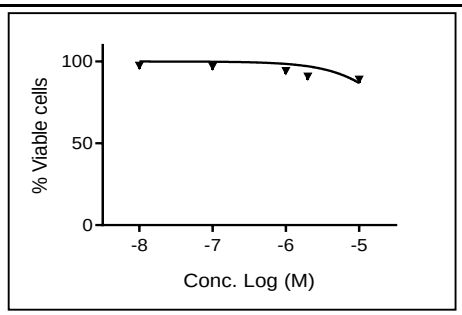
AZD1480 (≤10 µM)	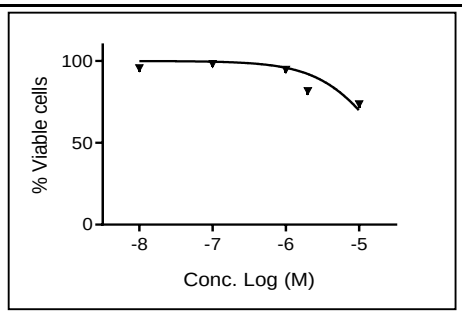

AZD4547 (≤10 μM)	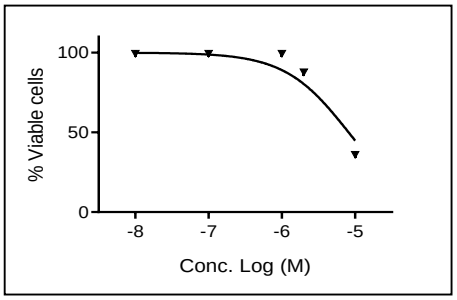
AZD7762 hydrochloride (≤1 μM)	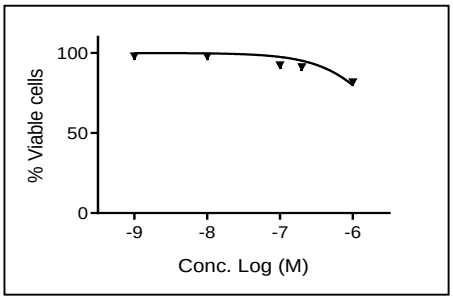
AZD8055 (≤10 μM)	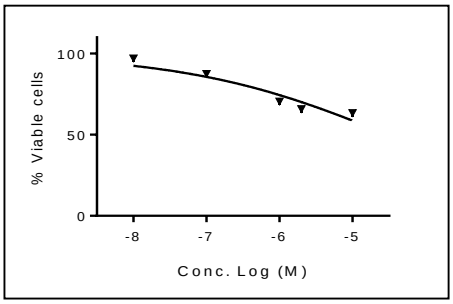
Barasertib (AZD1152-HQPA|AZD2811) (≤1 μM)	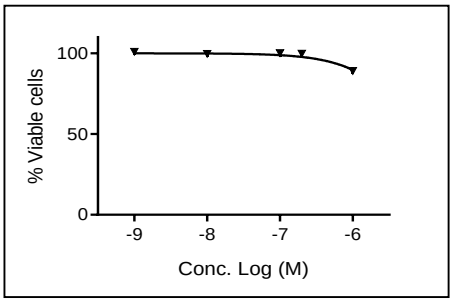
BGJ398 (NVP-BGJ398) (≤1 μM)	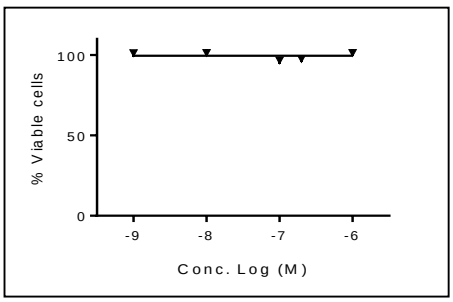

BI 2536 (≤1 µM)	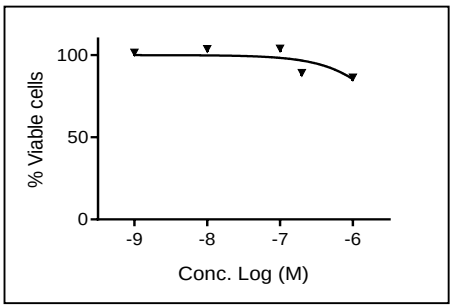
Binimetinib (MEK162, ARRY-162, ARRY-438162)(≤ 1 µM)	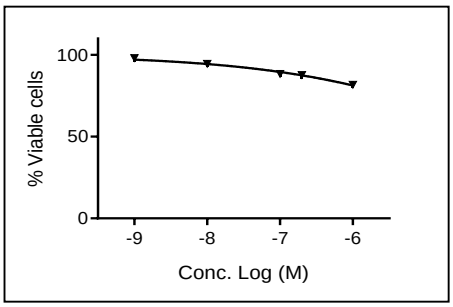
BMS-754807 (≤10 µM)	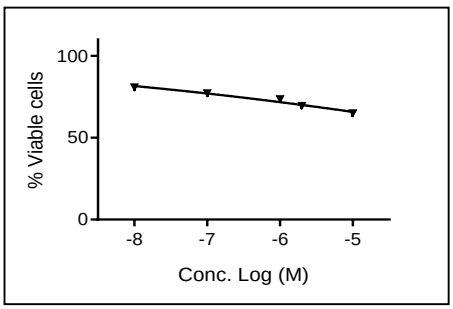
BMS-911543 (≤10 µM)	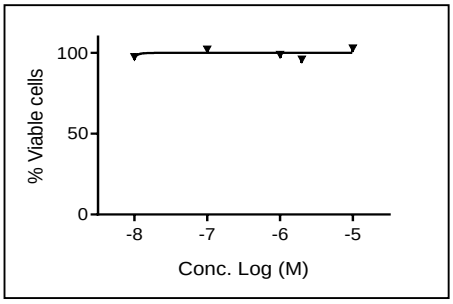
Bosutinib (SKI-606) (≤10 µM)	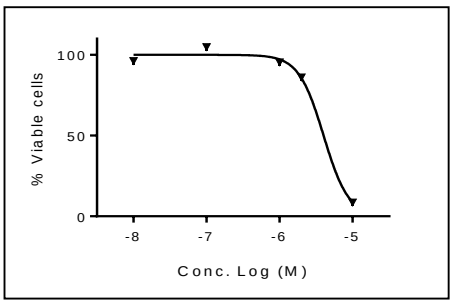

Brivanib (BMS-540215)(≤1 μM)	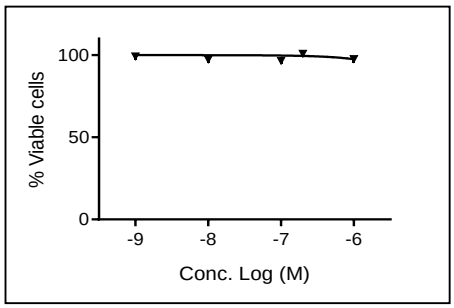
Buparlisib (BKM120, NVP-BKM120) (≤10 μM)	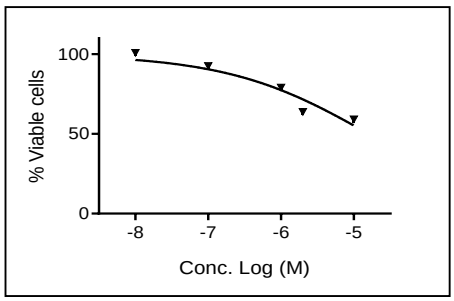
Cabozantinib (XL184, BMS-907351)(≤1 μM)	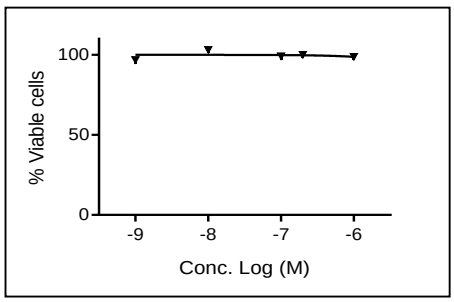
Canertinib (CI-1033) (≤10 μM)	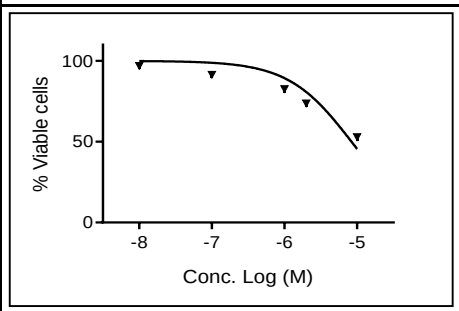
Cediranib (AZD2171, Recentin) (≤1 μM)	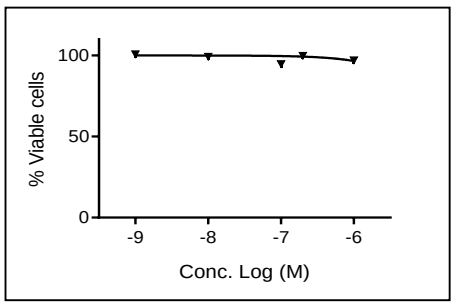

CP-724714 (≤10 µM)	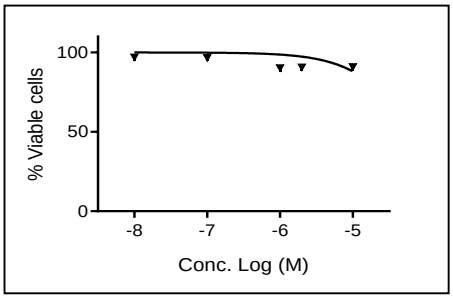
Crenolanib (CP-868596) (≤10 µM)	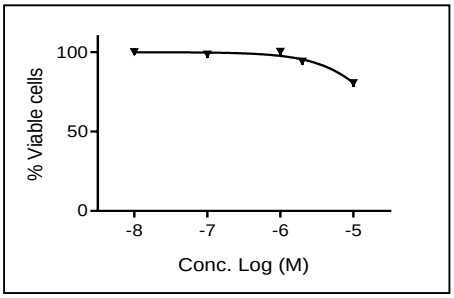
Crizotinib (PF-02341066) (≤1 µM)	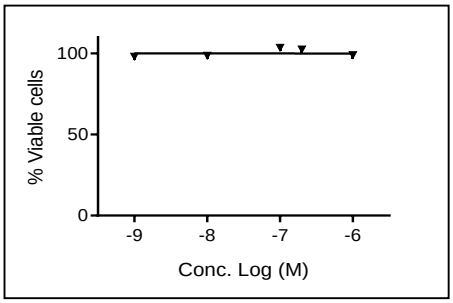
CUDC-101 (≤10 µM)	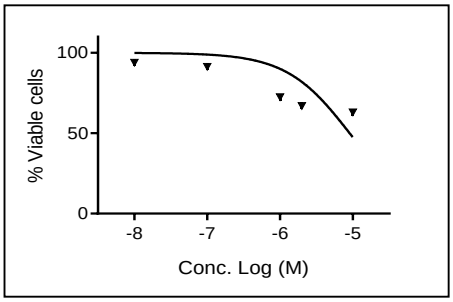
Dabrafenib Mesylate (≤ 2,5 µM)	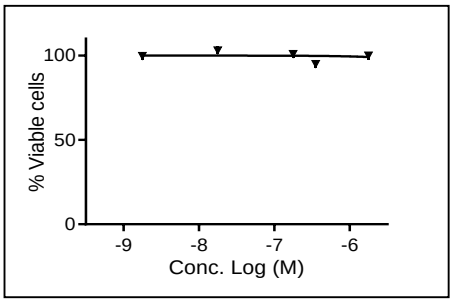

Dacomitinib (PF299804, PF299) (≤ 1 µM)	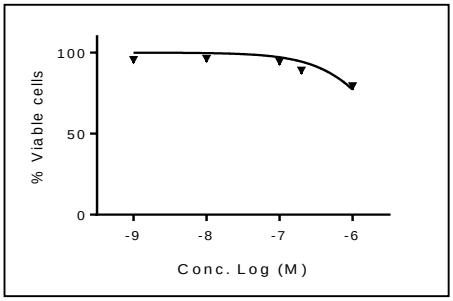
Dactolisib (BEZ235, NVP-BEZ235) (≤10 µM)	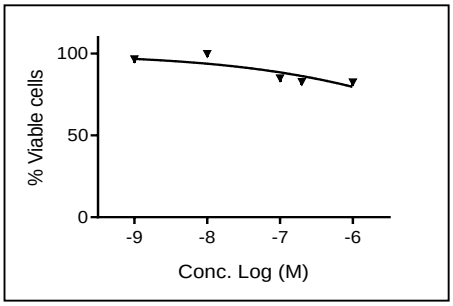
Danusertib (PHA-739358) (≤10 µM)	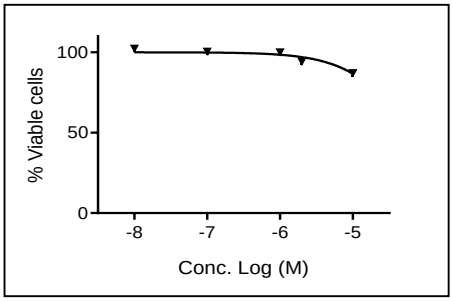
Dasatinib (≤ 1 µM)	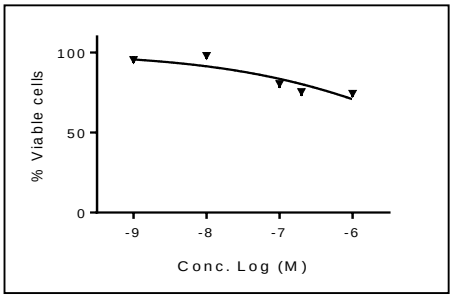
Dinaciclib (SCH727965) (≤1 µM)	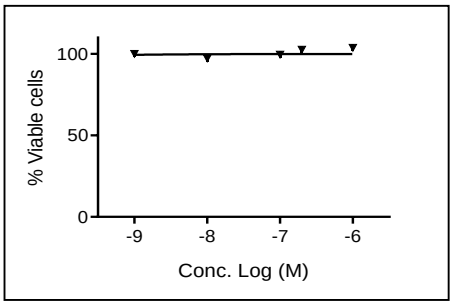

Doramapimod (BIRB 796) (≤10 µM)	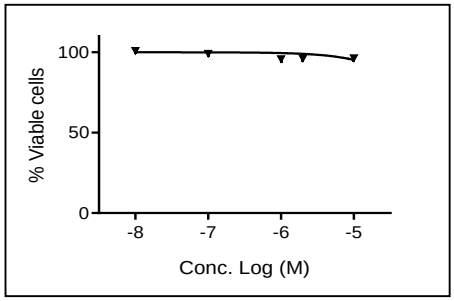
Dovitinib (TKI-258, CHIR-258) (≤10 µM)	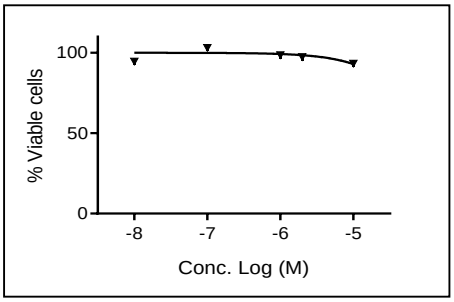
Enzastaurin (LY317615) (≤10 µM)	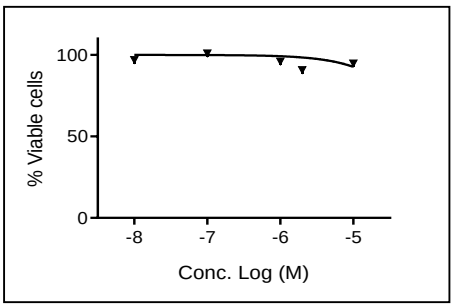
Erlotinib (≤10 µM)	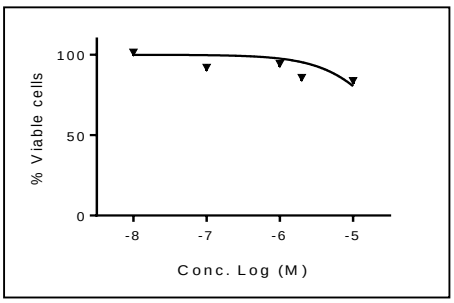
Everolimus (RAD001)(≤ 1 µM)	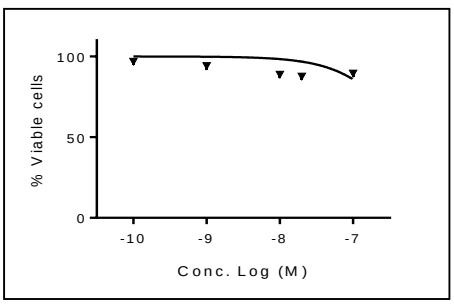

Fasudil (HA-1077) (≤50 µM)	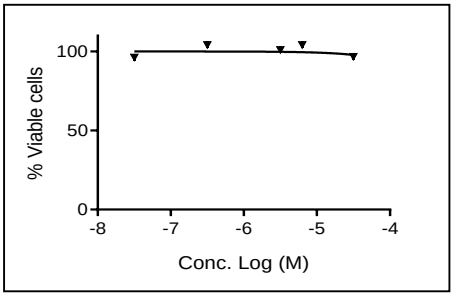
Fedratinib (SAR302503, TG101348) (≤10 µM)	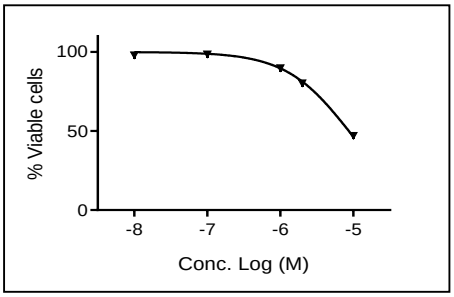
Flavopiridol (Alvocidib) (≤10 µM)	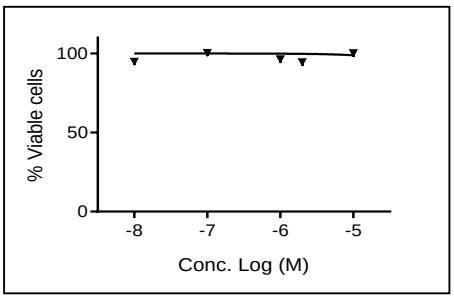
Foretinib (XL880)(≤10 µM)	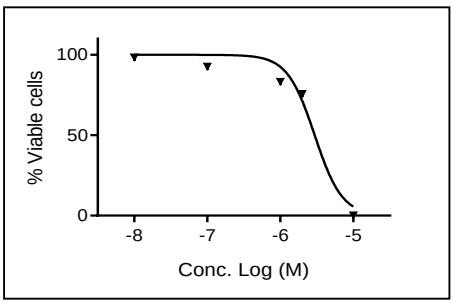
Fostamatinib (R935788) (≤2,5 µM)	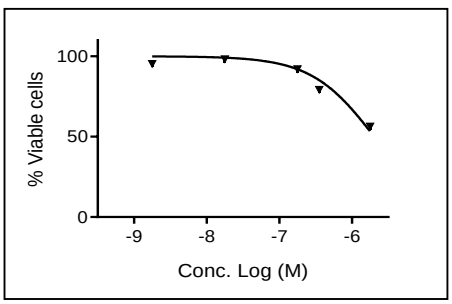

Galunisertib (LY2157299) (≤10 µM)	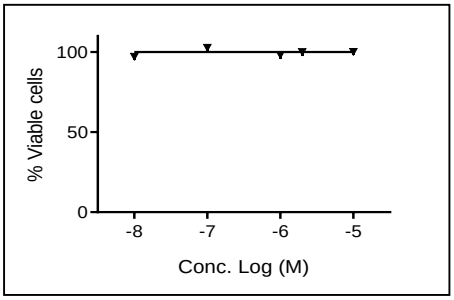
Gandotinib (LY2784544) (≤10 µM)	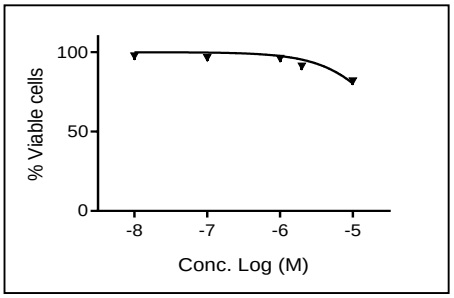
GDC-0879 (≤10 µM)	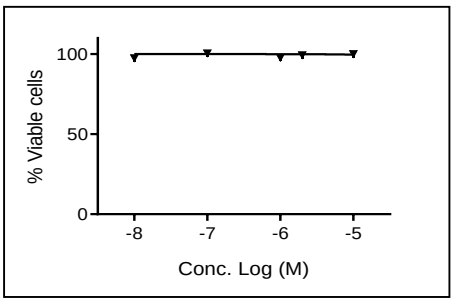
Gefitinib (ZD1839)(≤ 10 µM)	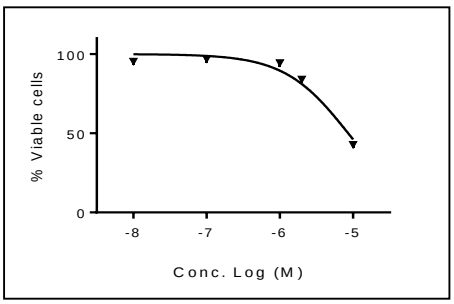
Glesatinib (MGCD265) (≤10 µM)	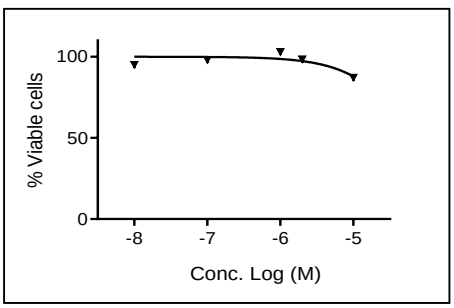

GSK1838705A (≤10 µM)	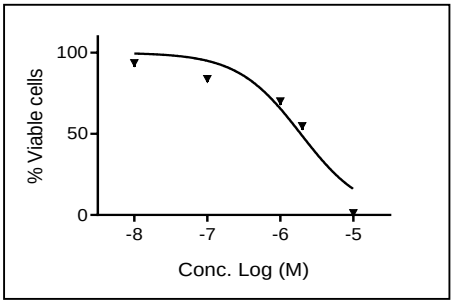
GSK2636771 (≤10 µM)	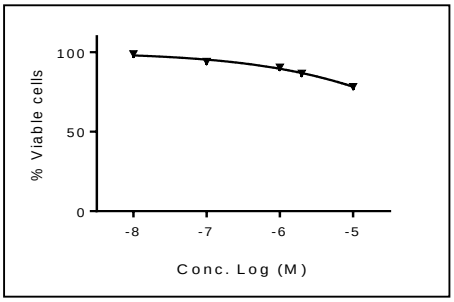
GSK269962 (≤10 µM)	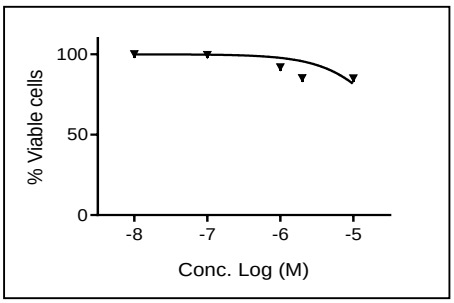
GSK461364A (≤10 µM)	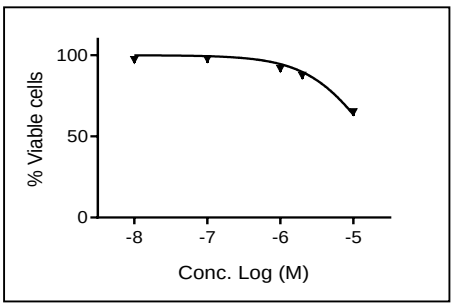
GSK650394 (≤10 µM)	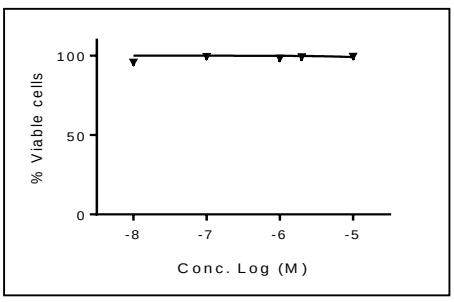

GW2580 (≤10 µM)	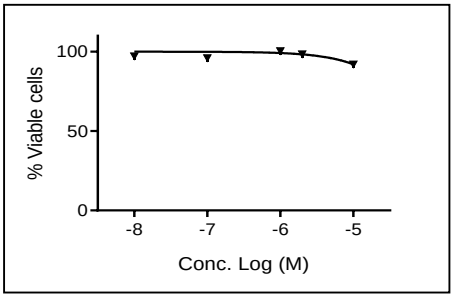
Ibrutinib (PCI-32765) (≤1 µM)	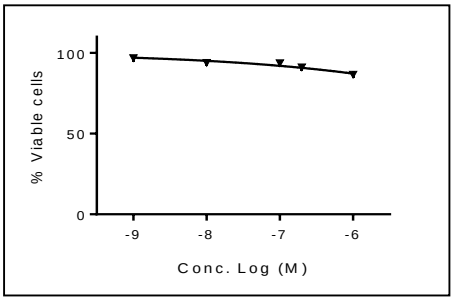
Idelalisib (CAL-101, GS-1101) (≤10 µM)	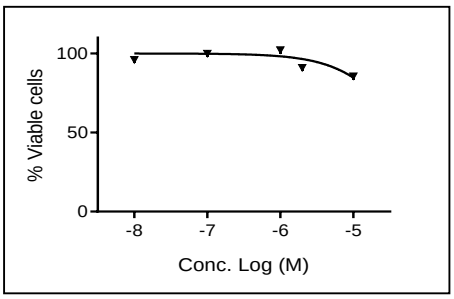
Imatinib (STI571)(≤ 10 µM)	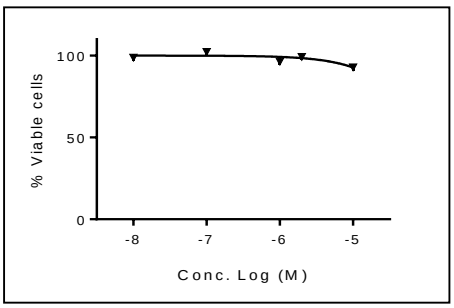
Ipatasertib (GDC 0068) (≤ 10 µM)	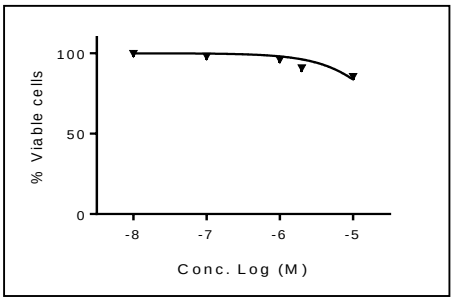

KW-2449 (≤10 µM)	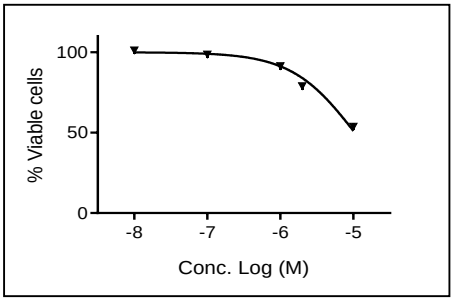
KX2-391 (≤10 µM)	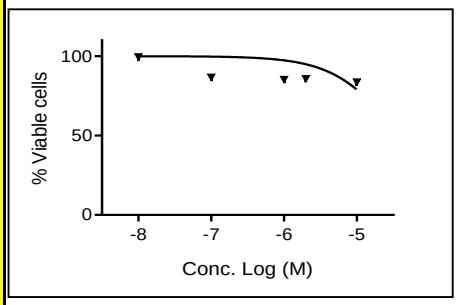
Lapatinib (≤ 1 µM)	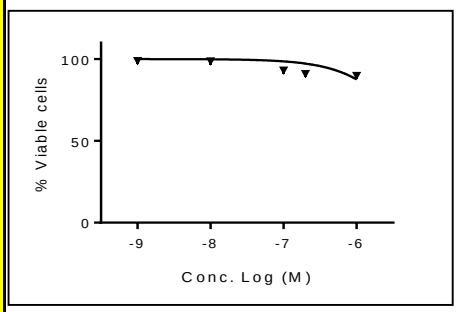
Lestauritinib (CEP701) (≤1 µM)	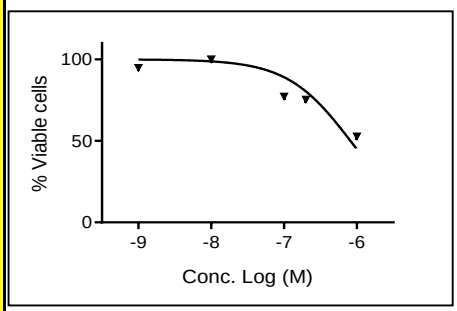
Linifanib (ABT-869) (≤1 µM)	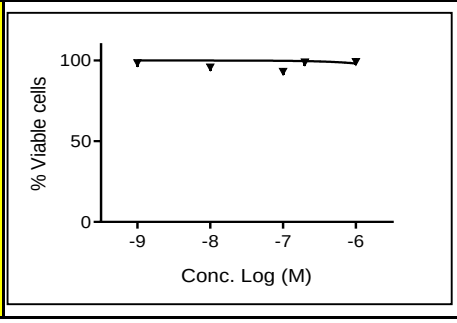

Linsitinib (OSI-906)(≤10 μM)	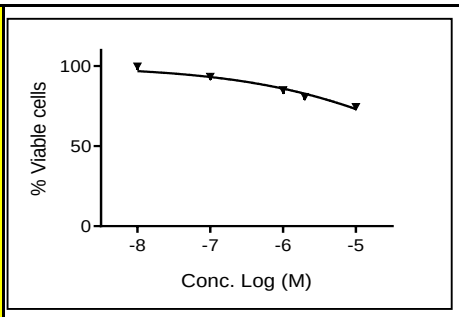
Masitinib (AB1010) (≤10 μM)	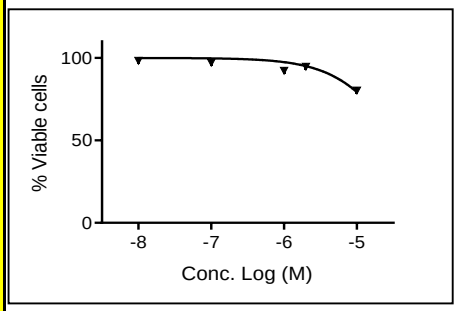
Midostaurin (PKC412) (≤ 10 μM)	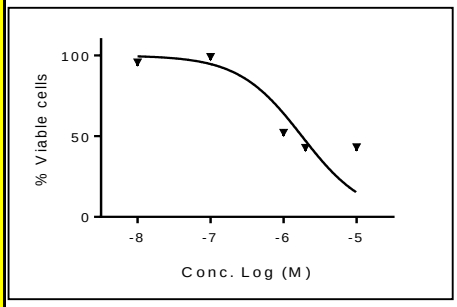
MK-2206 (≤ 1 μM)	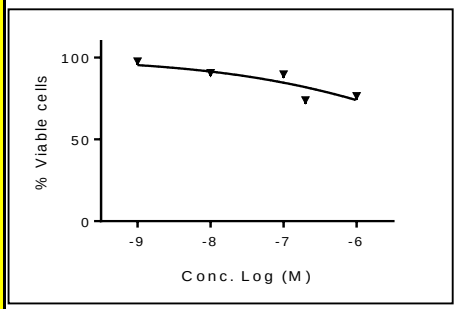
MLN-8054 (≤10 μM)	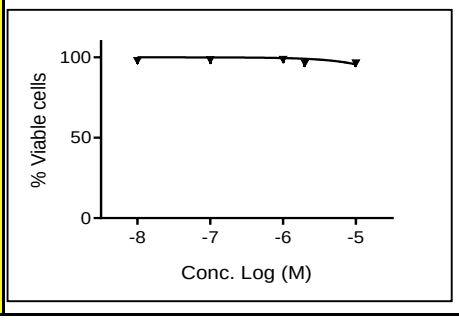

Momelotinib (CYT387) (≤10 µM)	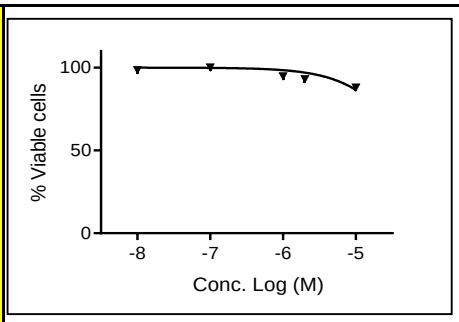
Motesanib Diphosphate (AMG-706) (≤50 µM)	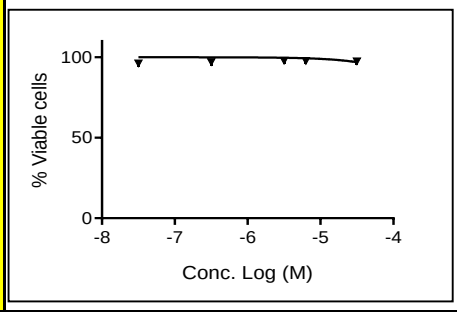
Neratinib (HKI-272) (≤ 1 µM)	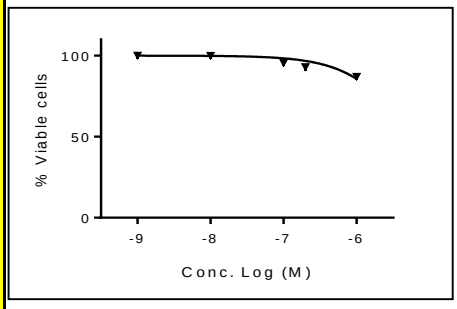
Nilotinib (AMN-107) (≤10 µM)	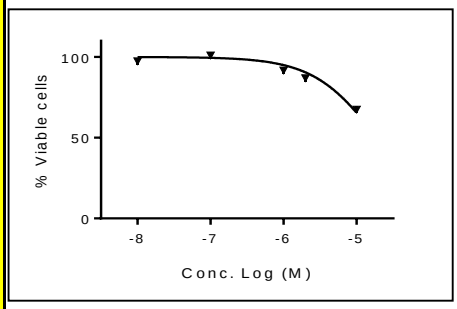
Nintedanib (BIBF 1120) (≤ 10 µM)	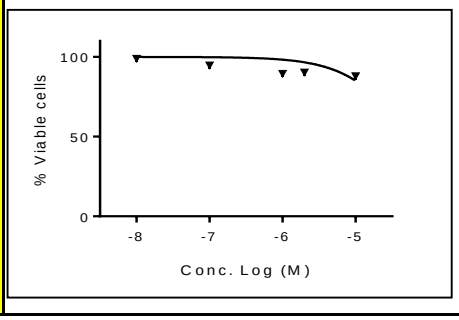

Omipalisib (GSK2126458, GSK458) (≤1 μM)	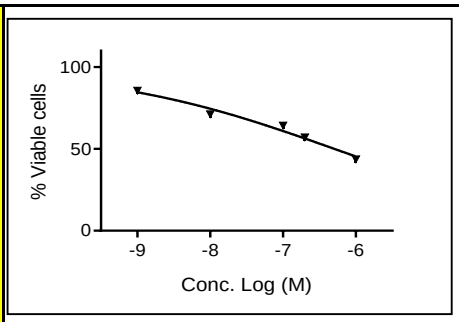
OSI-027 (≤10 μM)	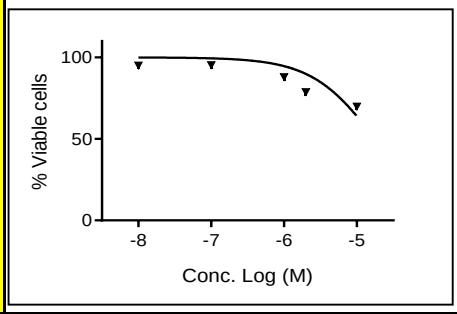
Palbociclib (PD-0332991) (≤10 μM)	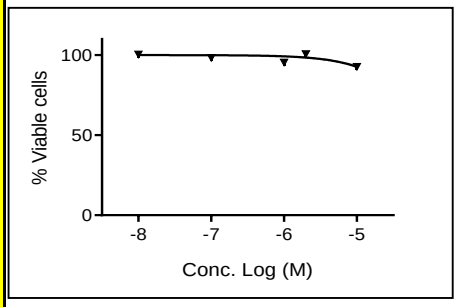
Pazopanib (≤10 μM)	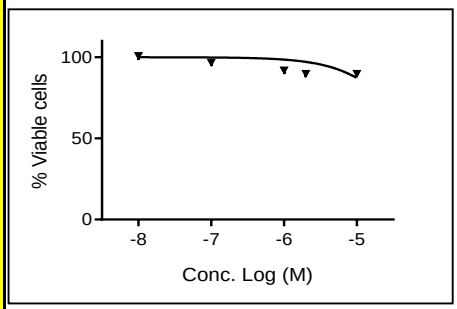
PD 184352 [CI-1040] (≤10 μM)	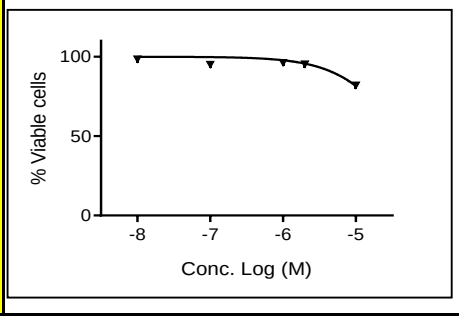

Pelitinib (EKB-569) (≤10 μM)	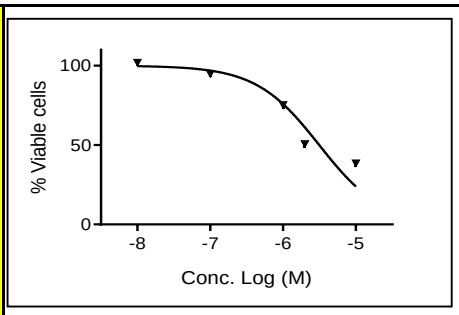
PF04691502 (≤10 μM)	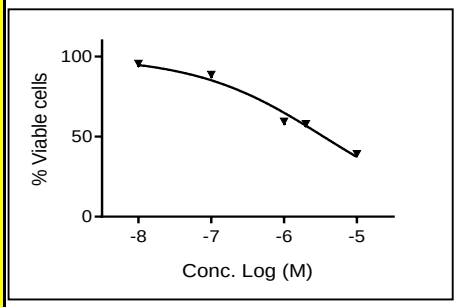
PF431396 (≤10 μM)	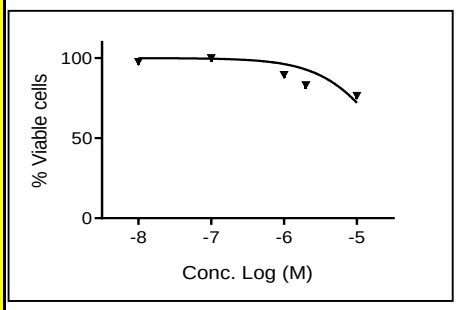
PF4708671 (≤10 μM)	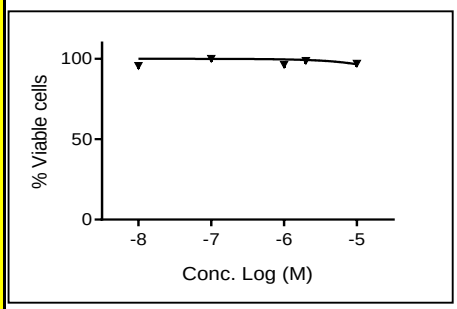
PF477736 (≤10 μM)	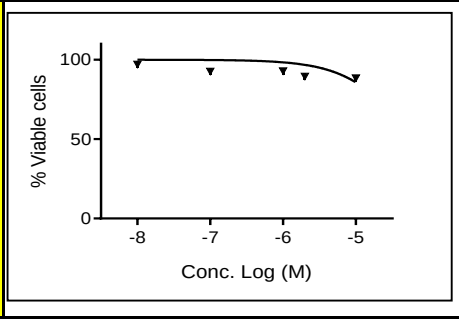

PF4800567 hydrochloride (≤10 µM)	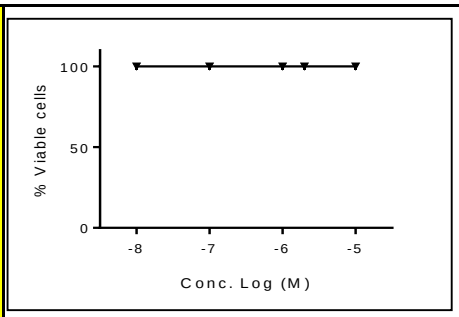
PF670462 (≤10 µM)	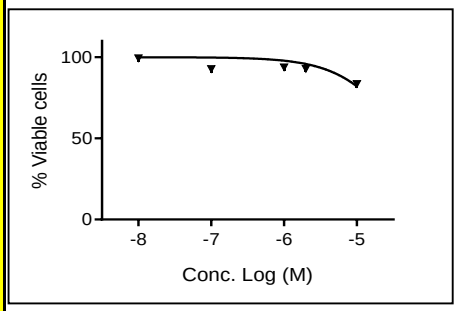
PHA-665752 (≤10 µM)	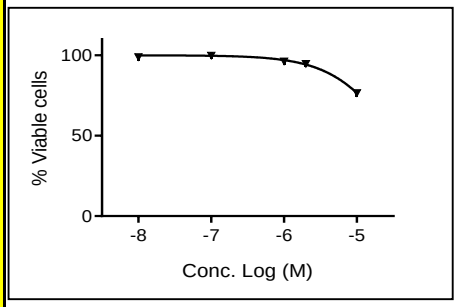
PI 103 (≤10 µM)	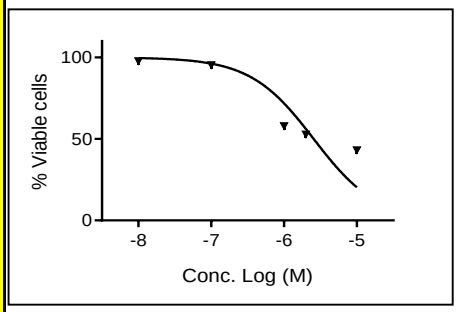
Pictilisib (GDC-0941) (≤10 µM)	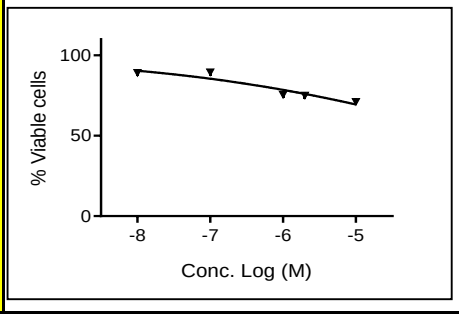

PIK75 (≤10 μM)	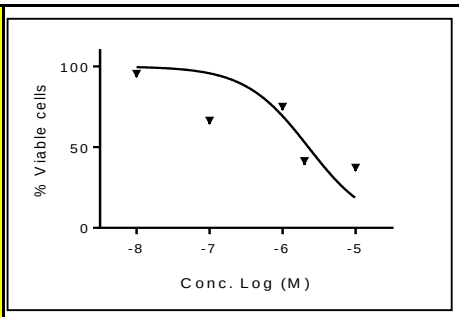
Pilaralisib (XL 147) (≤10 μM)	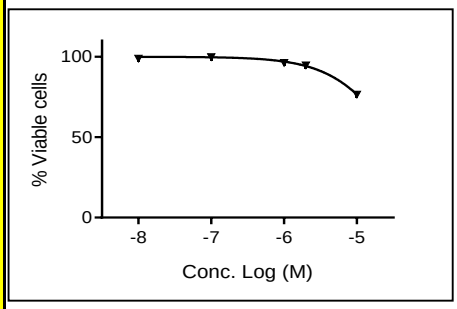
Pimasertib (AS-703026) (≤10 μM)	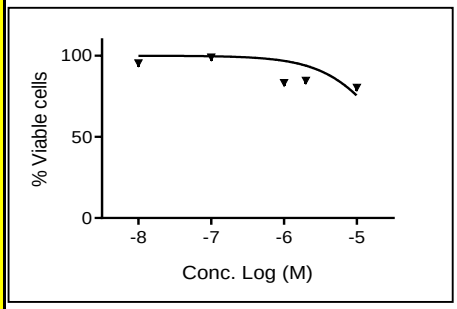
PLX-4720 (≤10 μM)	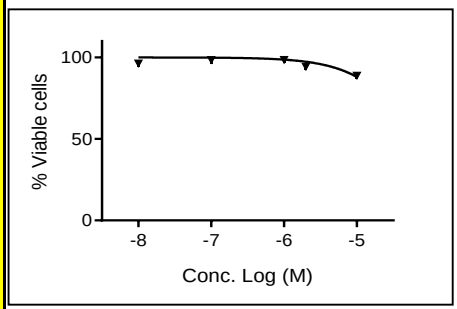
Ponatinib (AP24534) (≤ 10 μM)	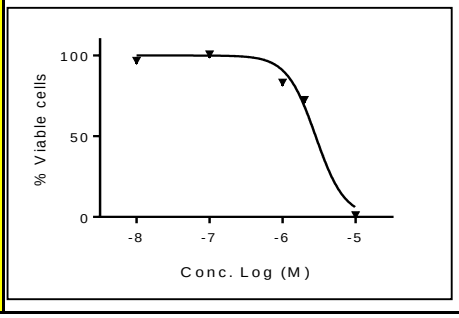

Quizartenib (AC220) (≤ 1 µM)	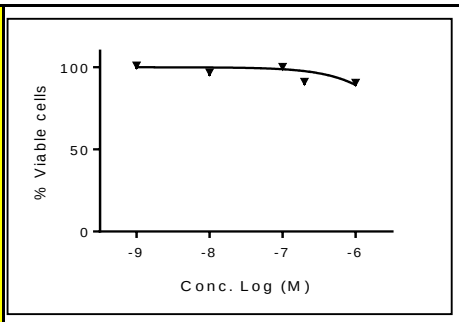
Rabusertib (LY2603618) (≤1 µM)	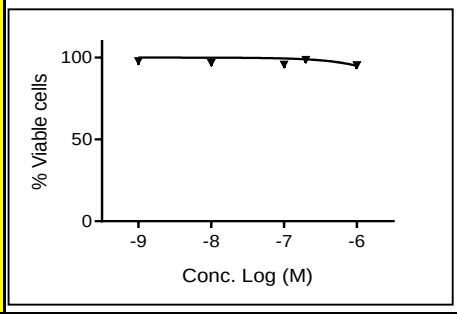
RAF265 (CHIR265)(≤10 µM)	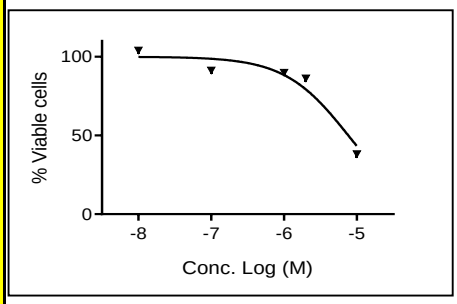
Ralimetinib (LY2228820) (≤10 µM)	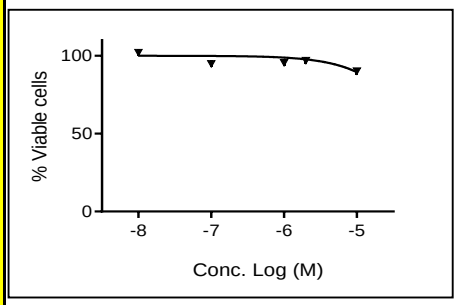
Rapamycin (Sirolimus) (≤ 1 µM)	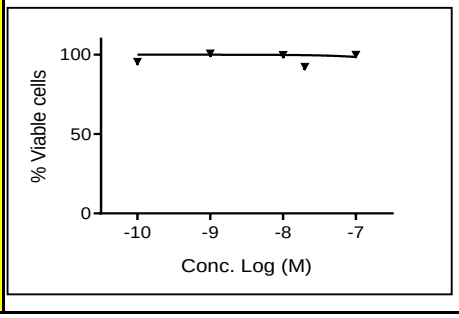

Rebastinib (DCC-2036) (≤1 μM)	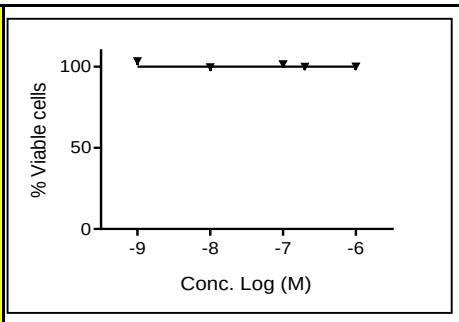
Refametinib (RDEA119, Bay 86-9766) (≤10 μM)	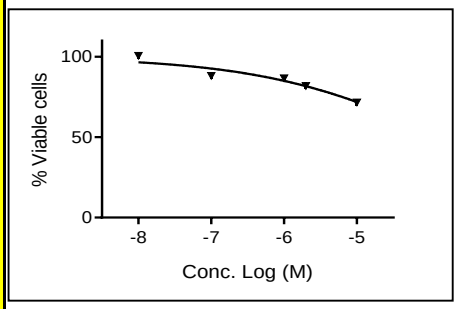
Regorafenib (BAY 73-4506) (≤10 μM)	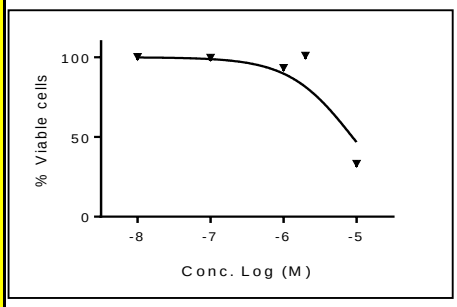
Roscovitine (Seliciclib,CYC202) (≤10 μM)	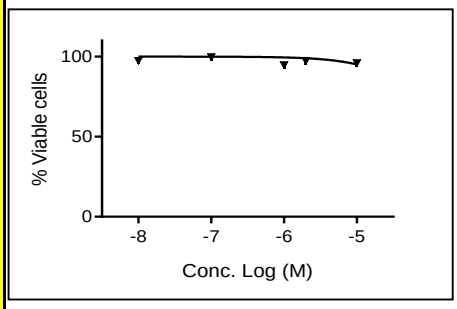
Ruboxistaurin (LY333531 HCl) (≤10 μM)	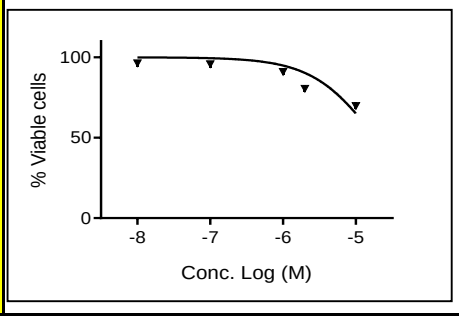

Ruxolitinib (INCB018424,) (≤10 µM)	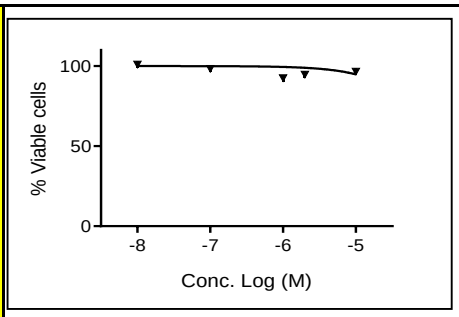
Sapanisertib (INK128) (MLN0128) (≤ 1 µM)	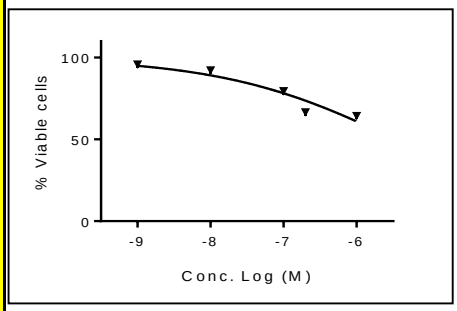
Saracatinib (AZD0530) (≤10 µM)	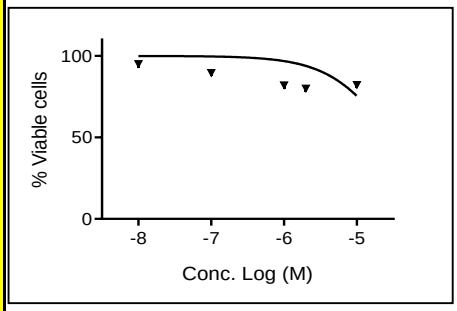
Selumetinib (AZD6244)(≤10 µM)	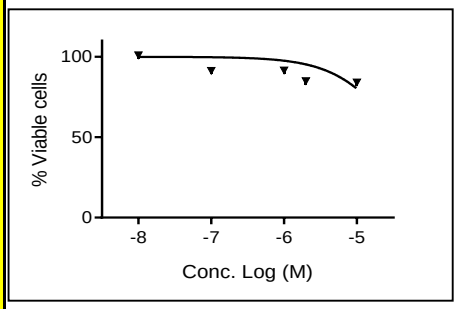
SGX-523 (≤10 µM)	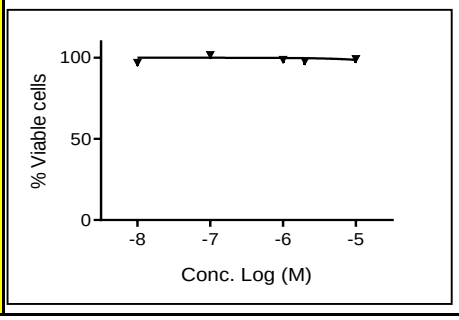

SNS-032 (BMS-387032) (≤10 μM)	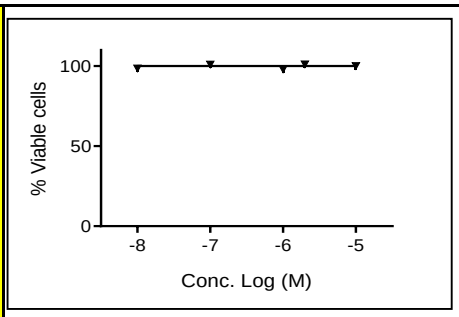
Sonolisib (PX866) (≤10 μM)	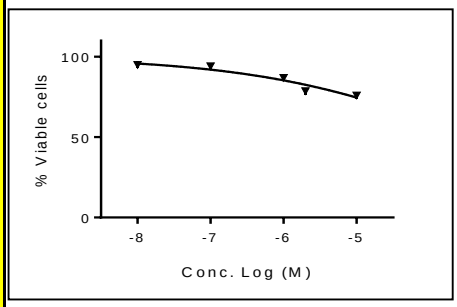
Sorafenib (≤ 1 μM)	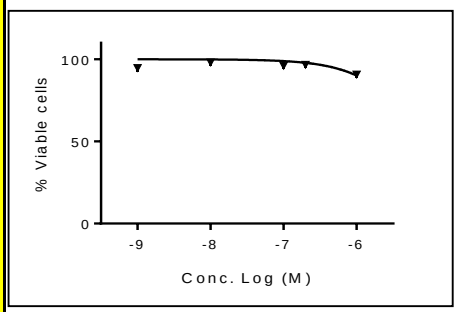
Sotrastaurin (≤10 μM)	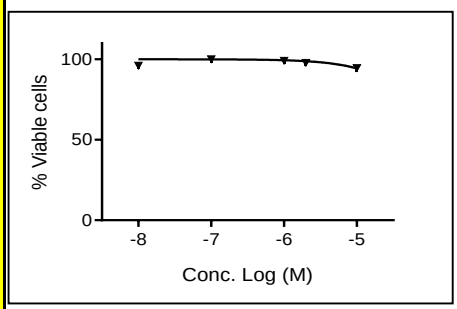
SP600125 (≤10 μM)	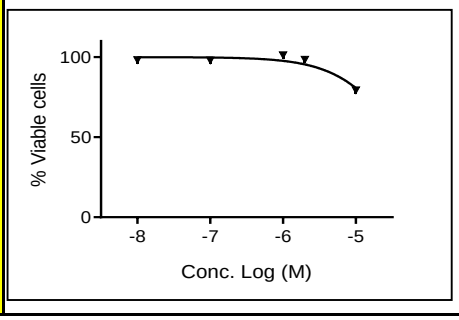

Staurosporine (≤10 μM)	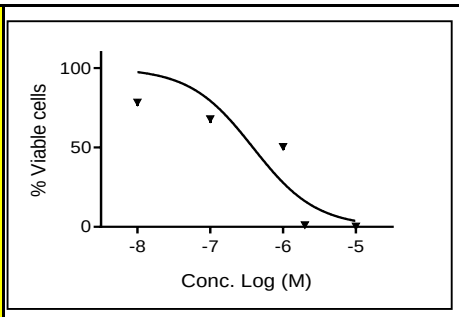
Sunitinib (≤ 1 μM)	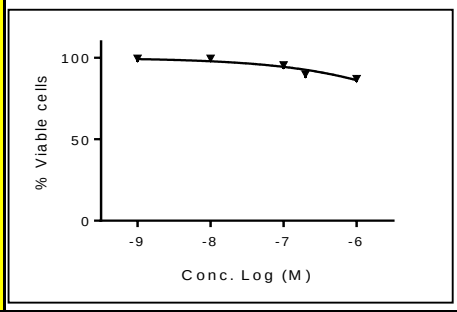
TAE-684 (≤10 μM)	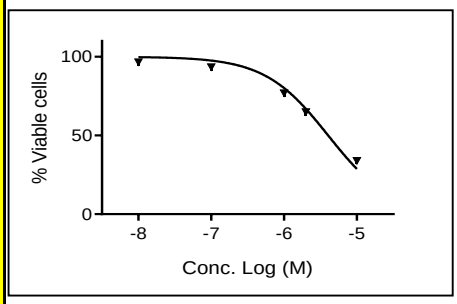
TAK-733 (≤10 μM)	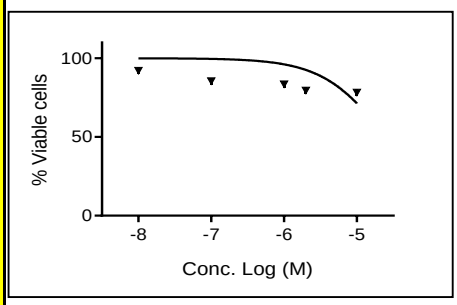
TAK901 (≤10 μM)	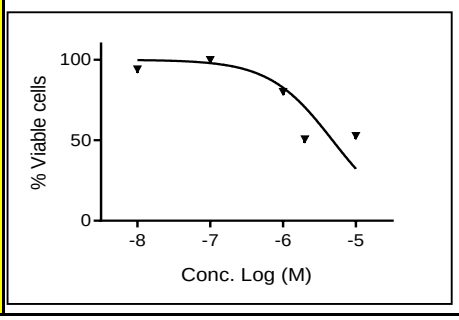

Tamatinib (R406) (≤10 μM)	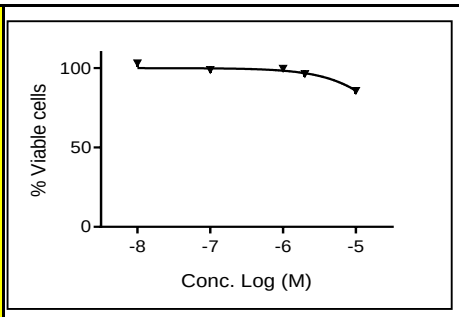
Tandutinib (MLN518) (≤10 μM)	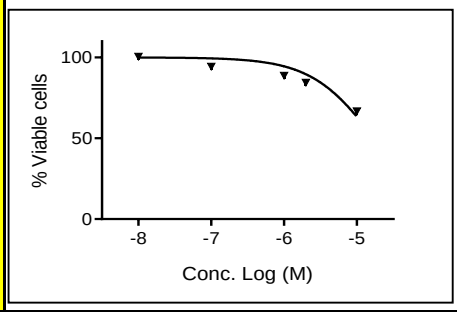
Tepotinib (EMD 1214063) (≤1 μM)	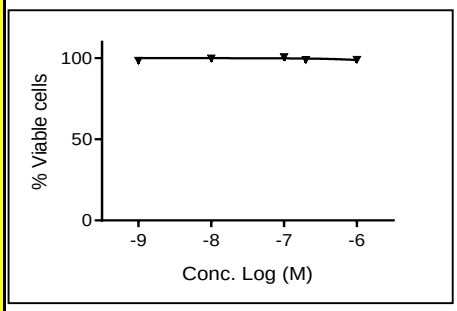
TG-100-115 (≤10 μM)	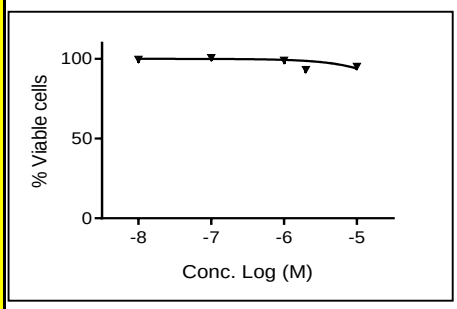
TGX-221 (≤10 μM)	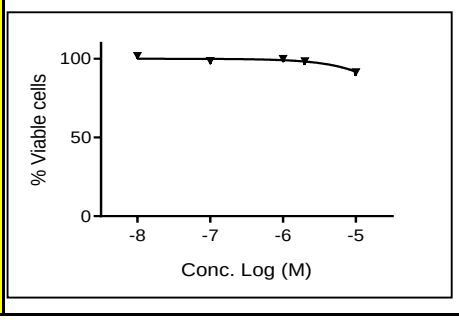

Tivantinib (ARQ 197) (≤10 μM)	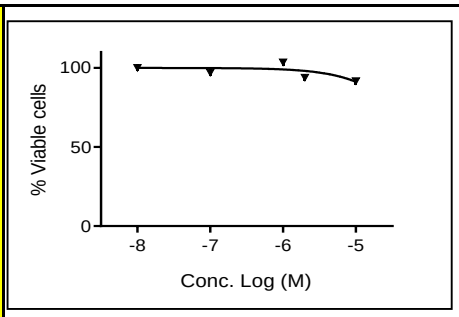
Tivozanib (AV-951) (≤10 μM)	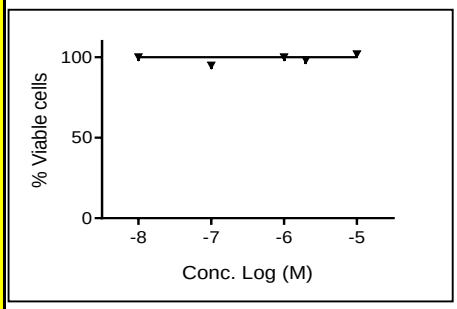
Tofacitinib (CP-690550,Tasocitinib) (≤ 5 μM)	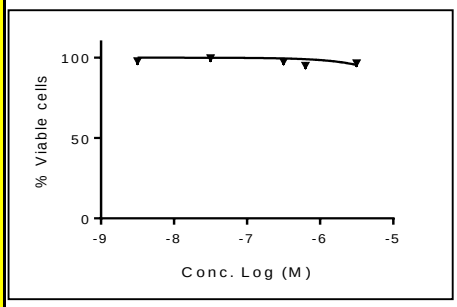
Torkinib (PP242)(≤10 μM)	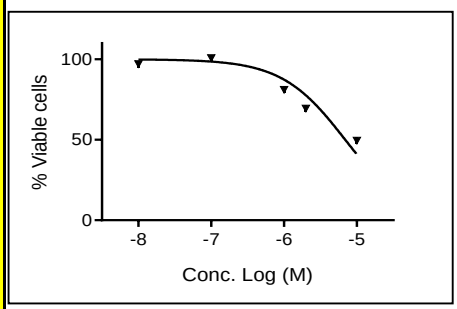
Tozasertib (VX-680, MK-0457) (≤10 μM)	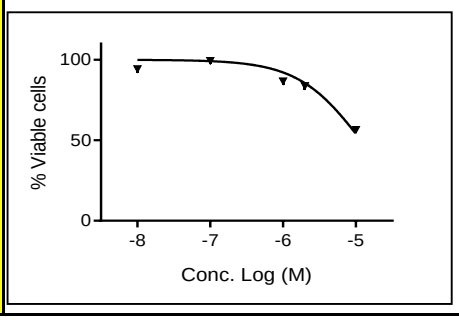

Trametinib (GSK1120212) (≤ 0,25 µM)	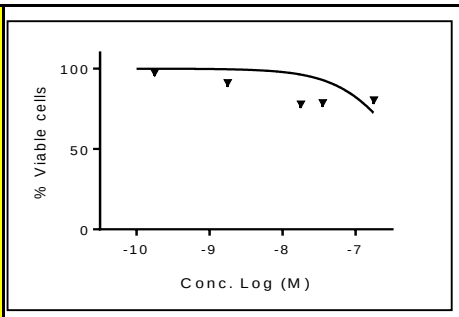
UCN-01 (≤10 µM)	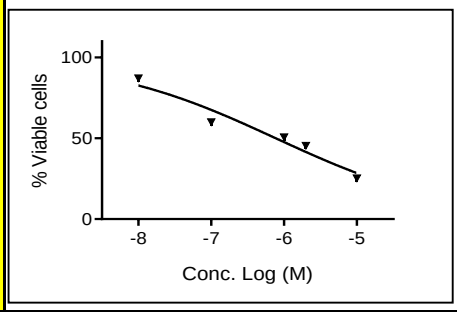
Vandertanib (≤ 1 µM)	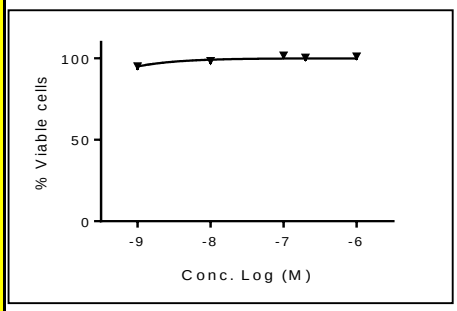
Vatalanib (PTK787) 2HCl (≤10 µM)	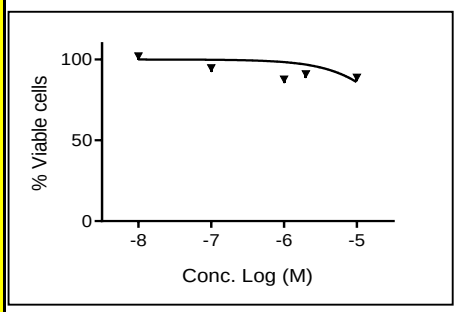
Vemurafenib (PLX4032, RG7204)(≤10 µM)	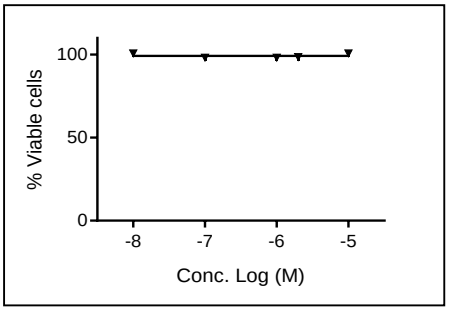

Vistusertib (AZD2014) (≤ 2,5 µM)	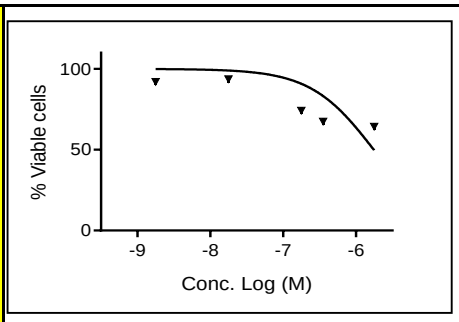
Volasertib (BI 6727) (≤10 µM)	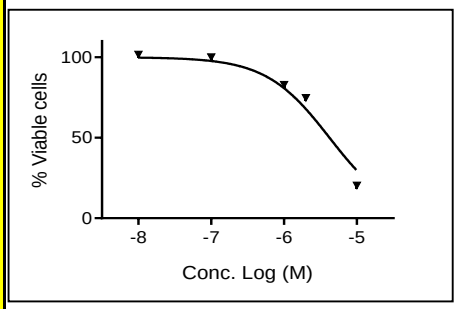
Voxtalisib (XL765, SAR245409) (≤10 µM)	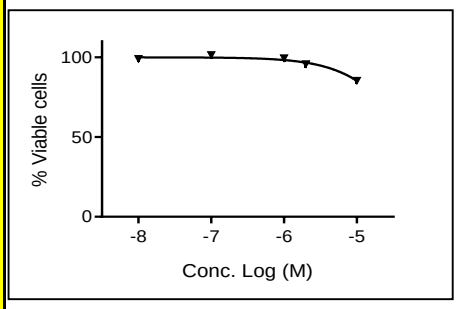
VX 11E (≤ 2,5 µM)	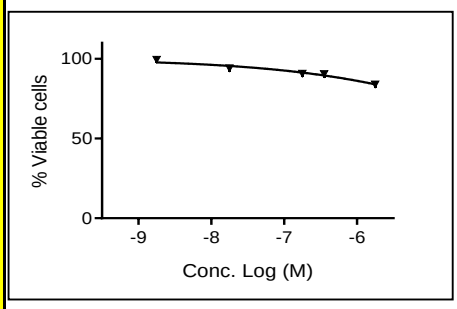
VX-745 (≤10 µM)	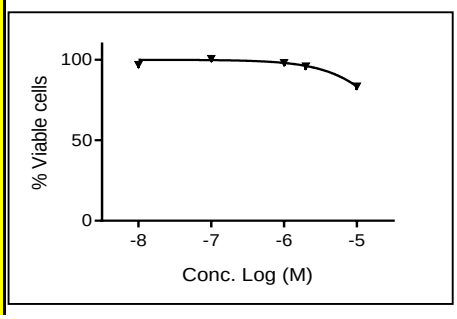

ZSTK474 (≤10 μM)	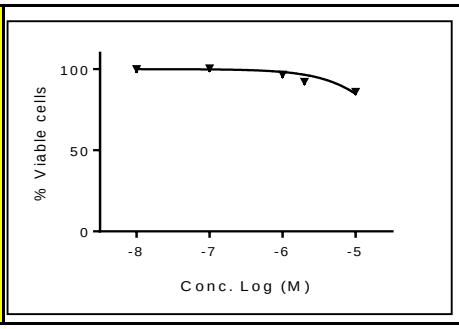

Table S2. DSS values, primary kinase targets and maximum concentration tested of all KIs included in the screen. The kinase targets of the compounds were extracted from the FIMM in-house Drug Target Commons (DTC) database (https://drugtargetcommons.fimm.fi/). Data is arranged in descending order according to DSS vlaues.

Kinase Inhibitor	DSS	Targets	Max Conc. Tested (nM)
Staurosporine	44.957	Several Kinases	10000
UCN-01	36.731	PKCbeta, PDK1, Chk, Cdk2	10000
PIK-75	25.300	PI3K	10000
Omipalisib	22.393	PI3K/mTOR	1000
Midostaurin	20.748	PKC, PKA, S6K and EGFR	10000
PF-04691502	19.320	PI3K/mTOR	10000
PI-103	19.210	PI3K	10000
GSK-1838705A	18.014	IGF1R, INSR, ALK	10000
BMS-754807	17.531	IGF1R	10000
Pelitinib	14.488	EGFR	10000
AZD8055	13.196	mTOR	10000
TAK-901	12.163	Aurora B	10000
TAE-684	12.039	ALK, Several Kinases	10000
CUDC-101	11.558	HDAC & EGFR, Her2	10000
(5Z)-7-Oxozeaenol	11.492	TAK1	10000
Apitolisib	10.959	PI3K/mTOR	10000
Ponatinib	10.717	Broad TK	10000
Foretinib	10.637	MET, VEGFR2	10000
Vistusertib (AZD2014)	10.430	mTOR, ATP-competitive	10000
Buparlisib	9.905	PI3K, pan-class I	10000
Pictilisib	9.507	PI3K, pan-class I	10000
Fostamatinib aq	8.839	Syk	2500
Torkinib (PP-242)	8.831	MTOR	10000
Volasertib	8.683	PLK1	10000
Canertinib	8.071	pan-ErbB	10000
Bosutinib	7.938	Abl, Src	10000
Sapanisertib (INK128)	6.815	mTOR	1000
Trametinib	6.636	MEK1/2	250
TAK-733	6.406	MEK	10000
Lestaurtinib	6.231	FLT3, JAK2, TrkA, TrkB, TrkC	1000
SAR302503	5.399	JAK2-selective	10000
RAF265	5.229	C-Raf	10000
AZD4547	5.132	FGFR	10000
Gefitinib	5.096	EGFR	10000
KW-2449	5.095	AURa AURb FLT3	10000
Saracatinib	4.928	Src, Abl	10000
Tozasertib	4.655	pan-Aurora	10000
Refametinib	4.652	MEK1/2	10000
KX2-391	4.630	non-ATP competitive Src	10000
Dasatinib	4.475	BCR/Abl, Src, Kit, EphR	1000
OSI-027	4.311	mTOR	10000

Linsitinib	4.237	IGF1R, IR	10000
Regorafenib	4.156	B-Raf, c-Kit, VEGFR2	10000
Sonolisib	4.051	PI3K, pan-class I, Irreversible	10000
Ruboxistaurin	3.598	PKCbeta	10000
Tandutinib	3.560	FLT3, PDGFR, KIT	10000
Pimasertib	3.438	MEK	10000
MK-2206	3.428	AKT	1000
AZD1480	2.808	JAK1/2, FGFR	10000
GSK-461364	2.728	PLK1	10000
Nilotinib	2.664	BCR/Abl	10000
PF 431396	2.657	FAK/PYK2	10000
MK1775	2.505	Wee1	10000
Dactolisib	2.169	PI3K/mTOR	1000
GSK2636771	1.863	p110beta selective PI3K	10000
Afatinib	1.834	EGFR	1000
Binimetinib	1.566	MEK	1000
Selumetinib	1.421	MEK	10000
Vatalanib	1.318	VEGFR-1 & -2	10000
GSK269962	1.244	ROCK1 and ROCK2	10000
Erlotinib	0.896	EGFR	10000
Pilaralisib	0.860	PI3K, Pan-class I	10000
Dacomitinib	0.840	pan-HER	1000
Gandotinib	0.665	JAK2	10000
VX-11E	0.653	ERK1 & 2	2500
Masitinib	0.567	KIT	10000
Crenolanib	0.555	PDGFRA and PDGFRB	10000
AZD7762	0.533	Chk1	1000
Everolimus	0.529	binds FKBP12, mTORC1	100
PD184352	0.414	MEK1/2	10000
SP600125	0.389	pan-JNK	10000
Nintedanib	0.368	VEGFR, PDGFR, FGFR	10000
GDC-0068	0.353	Akt	10000
Idelalisib	0.348	PI3K, p110 δ-selective	10000
PHA-665752	0.331	MET	10000
PF-670462	0.269	CK1epsilon and CK1delta	10000
BI 2536	0.233	PLK1	1000
Sunitinib	0.216	Broad TK	1000
ZSTK474	0.210	p110gamma selective PI3K	10000
Voxtalisib	0.153	mTOR/PI3K	10000
Tamatinib	0.109	Syk	10000
Axitinib	0.105	VEGFR, PDGFR, KIT	10000
Danusertib	0.103	Aurora, Ret, TrkA, FGFR-1	10000
PF-00477736	0.066	Chk1	10000
Neratinib	0.062	EGFR	1000
Ibrutinib	0.025	Btk	1000

Momelotinib	0.023	JAK1 & 2	10000
VX 745	0.013	p38MAPK	10000
MGCD-265	0.009	MET, VEGFR-1, -2, -3, RON, TIE2	10000
PLX-4720	0.008	BRAF	10000
Pazopanib	0.002	VEGFR	10000
Dabrafenib	0	B-Raf(V600E)	2500
GSK650394	0	SGK1 & 2	10000
Quizartinib	0	FLT3	1000
Vemurafenib	0	B-Raf(V600E)	10000
Tofacitinib	0	JAK3, JAK2(V617F)	5000
PF-4800567	0	CK1epsilon	10000
Ralimetinib	0	p38MAPK	10000
NVP-BGJ398	0	FGFR	1000
BMS-911543	0	JAK2	10000
Palbociclib	0	Cdk (Cdk4/6)	10000
Seliciclib	0	CDK2/7/9	10000
Doramapimod	0	p38	10000
Tivantinib	0	MET	10000
Dinaciclib	0	CDK	1000
Rebastinib	0	Allosteric ABL, FLT3, TIE2, TRKA	1000
Alisertib	0	Aurora A	10000
Motesanib	0	VEGFR, PDGFR, Ret, Kit	10000
Fasudil	0	Rho kinase, PKA, PKG, PRK, prodrug	50000
AZD1152-HQPA	0	Aurora B	1000
Rapamycin (Sirolimus)	0	binds FKBP12, mTORC1	100
TGX-221	0	p110beta selective PI3K	10000
Cediranib	0	KDR/Flt/VEGFR	1000
Vandetanib	0	VEGFR,EGFR, RET	1000
Cabozantinib	0	VEGFR2, Met, FLT3, Tie2, Kit and Ret	1000
Rabusertib	0	Chk1	1000
Sorafenib	0	B-Raf, FGFR-1, VEGFR-2-3, KIT	1000
Alvocidib	0	Cdk	10000
MLN-8054	0	AURa AURb FLT3 KIT (PDGFR)	10000
SNS-032	0	Cdk	10000
Tivozanib	0	VEGFR1, 2, 3, c-Kit, PDGFRB	10000
Imatinib	0	Abl, Kit, PDGFRB	10000
Crizotinib	0	ALK, c-Met	1000
EMD1214063	0	c-Met	1000
PF-04708671	0	p70S6K	10000
GDC-0879	0	BRAF(V600E)	10000
Ruxolitinib	0	JAK1&2	10000
Galunisertib	0	TGF-B/Smad	10000
Dovitinib	0	FGFR	10000

CP-724714	0	EGFR ERBB2	10000
GW-2580	0	CSF1R	10000
Sotrastaurin	0	PKC	10000
Enzastaurin	0	PKCbeta	10000
AT9283	0	Aurora A & B, Jak2, Flt, Abl	1000
Linifanib	0	VEGFR, PDGFR, CSF-1R, FLT3	1000
Lapatinib	0	HER2, EGFR	1000
Brivanib	0	VEGFR	1000
AZ 3146	0	Mps1 kinase (TTK)	10000
SGX-523	0	MET	10000
TG100-115	0	PI3K gamma/delta	10000

Table S3. Effect of selective PI3K. IGF1R. mTOR and dual PI3K/mTOR on AK levels at 24h incubation time. Neonatal cardiomyocytes were treated with 4 different concentrations of each inhibitor for 24 hours. At the end of experiment. media samples were collected for the toxilight assay. Data are arranged in descending order according to AK levels. Data are represented as mean *$p < 0.05$; **$p < 0.01$; ***$p < 0.001$; (Dunnett's test). IGF1R (Insulin Growth Factor 1 Receptor). mTOR (Mammalian Target of Rapamycin) and PI3k (Phosphoinositide 3-Kinase).

Inhibitor	Max AK release at 24h (folds vs control)	PI3K	mTOR	IGF1R
NVP-AEW541	**4.96 (***)**			•
Omipalisib/GSK2126458/ GSK458	**3.80 (***)**	•	•	
PI-103	**2.61 (***)**	•	•	
PKI402	**2.09 (***)**	•	•	
BMS754807	**1.95 (***)**			•
PF04691502	**1.76 (***)**	•	•	
PIK75	**1.69 (***)**	•		
Apitolisib	**1.69 (***)**	•	•	
BKM120	**1.68 (***)**	•		
GDC0941	**1.61 (***)**	•		
pp242	**1.43 (**)**		•	
XL147	**1.37 (***)**	•		
OSI-027	**1.14 (ns)**		•	
GSK1838705A	**1.12 (ns)**			•
INK128	**1.09 (ns)**		•	
GSK1904529A	**1.02 (ns)**			•
Vistusertib	**1.01 (ns)**		•	
AZD8055	**1.00 (ns)**		•	
Lisitinib	**1.00 (ns)**			•

Figure S1.

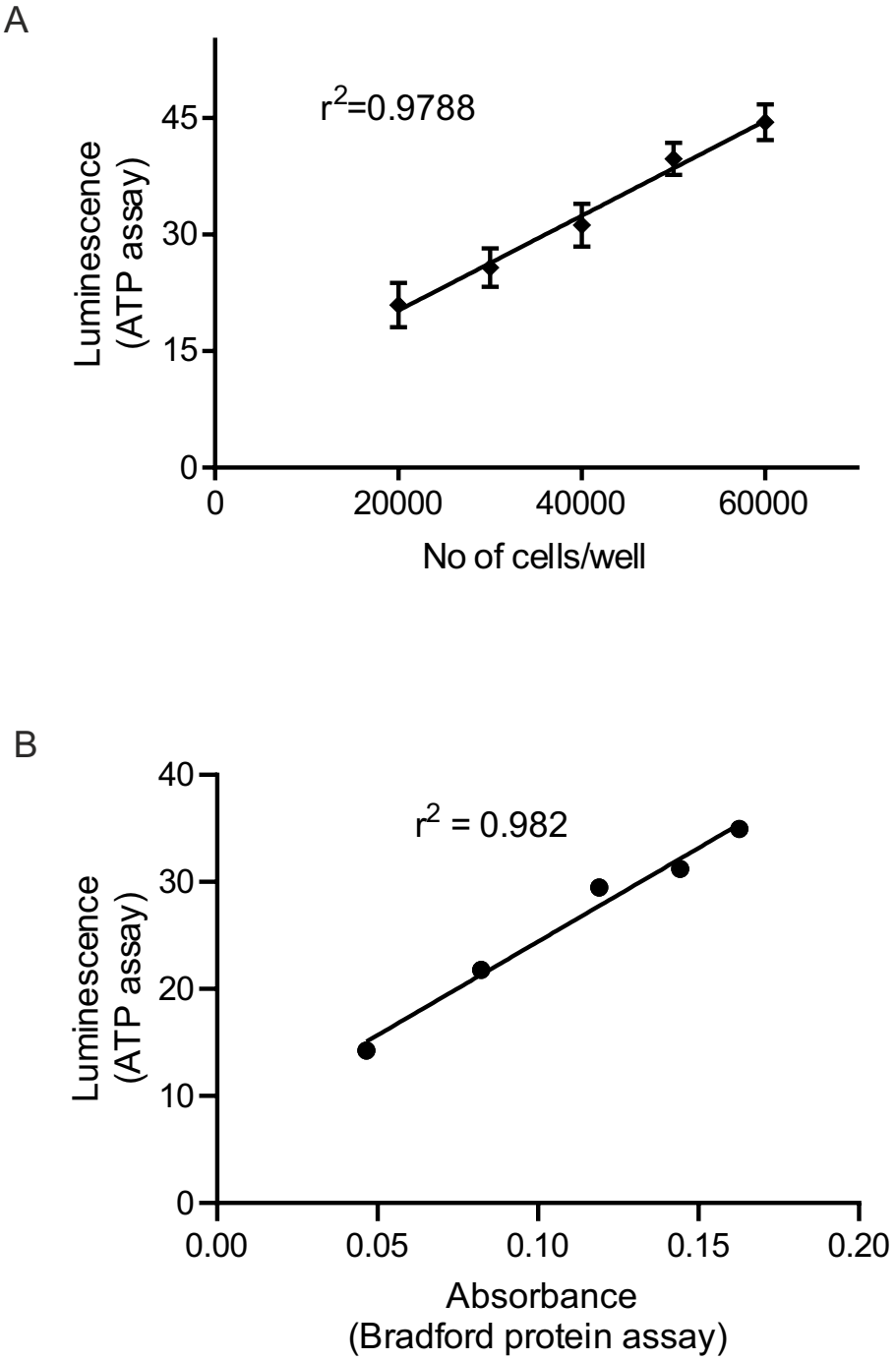

Supplementary Figure 1. Validation of ATP assay. A, Correlation of cell density and relative luminescence using ATP assay. Neonatal rat cardiomyocytes were plated onto 96-well plate at the density of 20 000 to 60 000 cells per well. 72 h after plating, cells were lysed, and ATP levels were measured. Shown are linear regression and Pearson's correlation coefficient between ATP levels and number of cells plated. B, Correlation of cardiomyocyte protein content and cellular ATP levels. Neonatal rat cardiomyocytes were plated at different cell densities. 24 h after plating, Cells were lysed with 0.1 M NaOH or ATP assay lysis reagent for determination of protein or ATP content respectively. Shown are linear regression and Pearson's correlation coefficient between ATP levels and protein content.

Figure S2.

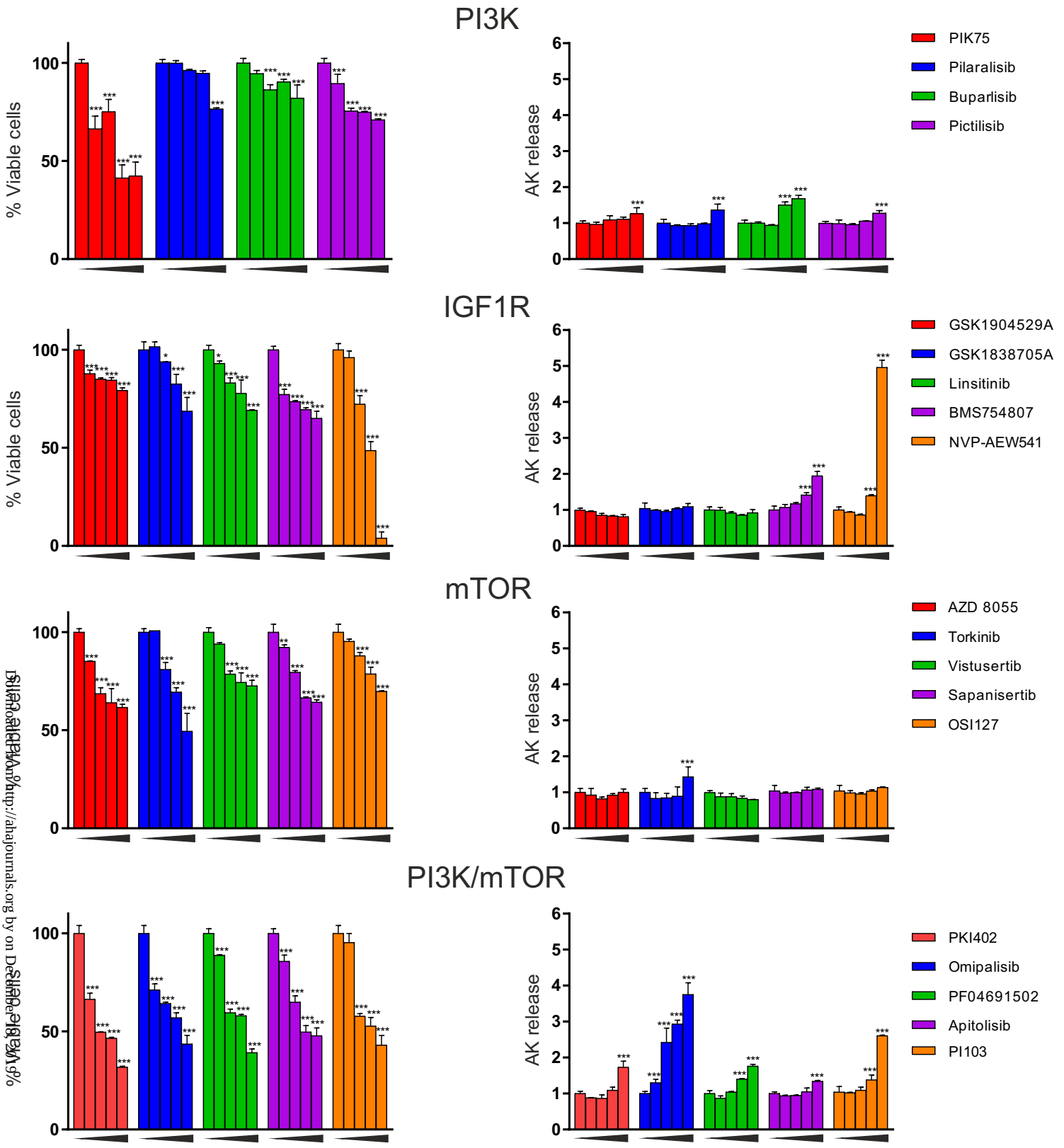

Supplementary Figure 2. Cardiomyocyte toxicity of selective inhibition of PI3K, IGF1R, mTOR and PI3K/mTOR. Neonatal rat cardiomyocytes were treated with 4 different concentrations of each inhibitor for 24 hours. Concentrations from left to right are 0.1, 1.0, 3.0, and 10 µM. At the end of experiment, medium samples were collected for adenylate kinase (AK) assay (right panels) and cells were lysed for measurement of ATP levels (left panels). Data from ATP assay is shown as percent of viable cells and AK assay as fold change in AK release vs control (DMSO). IGF1R (Insulin Growth Factor 1 Receptor), mTOR (Mammalian Target of Rapamycin) and PI3K (Phosphoinositide 3-Kinase). Data are presented as mean±SD *p < 0.05; **p < 0.01; ***p < 0.001; (Dunnett's test).

Figure S3.

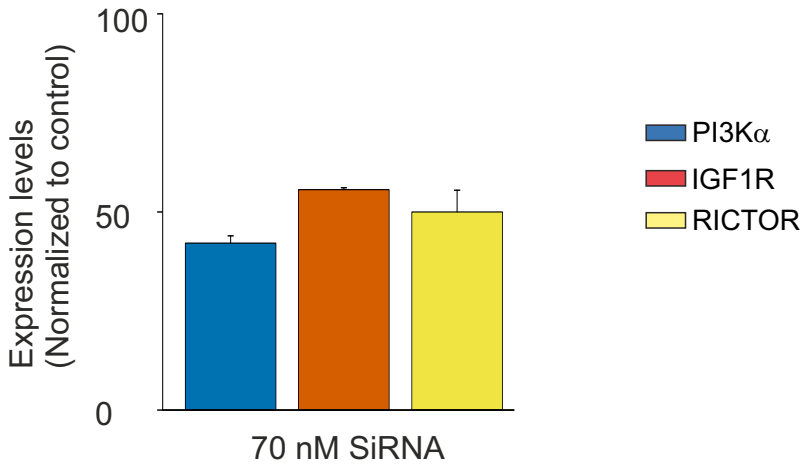

Supplementary figure 3. qPCR analysis of PI3Kα, IGF1R and RICTOR mRNA levels.Neonatal rat cardiomyocytes were transfected with 70 nM siRNAs targeting PI3Kα, IGF1R or RICTOR.